

THESIS ON MECHANICAL ENGINEERING E80

**Light-Weight Multicopter  
Structural Design for Energy Saving**

DMITRI ALEKSANDROV

**TUT**  
**PRESS**

TALLINN UNIVERSITY OF TECHNOLOGY  
Faculty of Mechanical Engineering  
Department of Mechatronics

**This dissertation was accepted for the defence of the degree of Doctor of Philosophy in Engineering on July 8, 2013.**

**Supervisor:** Associate Professor Igor Penkov,  
Department of Mechatronics, TUT

**Opponents:** Professor Janis Viba,  
Institute of Mechanics, Riga Technical University, Latvia

Rector Jaan Tamm,  
Estonian Aviation Academy, Estonia

Defense of the thesis: August 26, 2013

Declaration:

*Hereby I declare that this doctoral thesis, my original investigation and achievement, submitted for the doctoral degree at Tallinn University of Technology has not been submitted for doctoral or equivalent academic degree.*

Dmitri Aleksandrov

Copyright: Dmitri Aleksandrov, 2013  
ISSN 1406-4758  
ISBN 978-9949-23-521-6 (publication)  
ISBN 978-9949-23-522-3 (PDF)

MEHHANOTEHNIKA E80

**Kergklassi multikopteri  
energiatarbe vähendamise  
konstruktsioonilised lahendused**

DMITRI ALEKSANDROV



# CONTENTS

LIST OF PUBLICATIONS .....	6
INTRODUCTION.....	7
ABBREVIATIONS .....	10
1. OVERVIEW OF THE LITERATURE .....	11
1.1 Flying types of mini UAVs .....	11
1.2 Optimization and energy saving of UAVs.....	17
2. DETERMINATION OF ONE ROTOR LIFTING FORCE .....	21
2.1 Theory of propeller lifting force .....	21
2.2 Lift force determination .....	26
2.3 Comparison of simulation and experiment results.....	32
2.4 Rotor pitch calculation .....	33
3. FINDING OPTIMAL WAY OF ROTOR USAGE .....	36
3.1 Coaxial rotors.....	36
3.2 Shrouded rotors .....	41
3.3 Comparison of multicopters with a different number of rotors.....	49
4. OPTIMAL DISTANCE BETWEEN ROTORS .....	56
4.1 Influence of distance between the rotors on the lifting force .....	56
4.2 Optimal distance determination .....	61
4.3 Methodology .....	67
CONCLUSIONS .....	71
REFERENCES .....	74
OTHER PUBLICATIONS .....	80
ACKNOWLEDGEMENTS .....	81
ABSTRACT .....	82
KOKKUVÕTE.....	84
CURRICULUM VITAE.....	86
ELULOOKIRJELDUS.....	87

## LIST OF PUBLICATIONS

1. Aleksandrov, D., Penkov, I., Optimization of lift force of mini quadrotor helicopter by changing of gap size between rotors, *Solid State Phenomena: Mechatronic Systems and Materials IV*, 2013, Vol. 198, 226 – 231.
2. Aleksandrov, D., Penkov, I., Increasing of power characteristics of mini UAV helicopter by changing of its geometrical parameters, *Machines Technologies Materials*, 2012, Vol. 6, 30 – 32.
3. Aleksandrov, D., Penkov, I., Optimal gap distance between rotors of mini quadrotor helicopter, *Proceedings of the 8th International Conference of DAAAM Baltic, Industrial Engineering*, Tallinn, Estonia, 19 – 21 April 2012, 251 – 255.
4. Aleksandrov, D., Penkov, I., Fluid flow optimization on semiautomatic code marker base, *Journal of Energy and Power Engineering*, 2012, Vol. 6, No. 6, 916 – 920.
5. Aleksandrov, D., Penkov, I., Axial displacements in ball screw mechanisms with two and four contact-point, *International Review of Mechanical Engineering*, 2011, Vol. 5, No. 7, 1213 – 1218.

# INTRODUCTION

## Background

In the last decades many autonomous and teleoperated vehicles in applications of robotics have been developed, including wheeled or tracked and legged vehicles. However, in many cases, ground vehicles have significant inherent limitations to access to the desired locations due to the characteristics of the terrain and the presence of obstacles that cannot be avoided. In these cases aerial vehicles are the natural way to approach the objective to obtain information or even to perform necessary actions such as the deployment of instrumentation [1]. Unmanned aerial vehicles (UAV) are widely used in various civil [2 – 4] and military [5] applications. These devices are sometimes named “drones”, which are programmed for autonomous flight and remotely piloted (RPV) by a ground control operator.

UAVs have a relatively long history. The first unmanned aircraft was a torpedo developed in 1915 for the US Navy, which was designed to fly to a specific location and drive into its target. In the Second World War, they were used as radio-controlled targets and for reconnaissance missions [6].

UAVs are capable of carrying out work under conditions where the surrounding environment is dangerous or not accessible to humans. They can carry out many military applications such as border patrol monitoring [7] for illegal immigrants and drug smugglers detection, uninhabited combat aerial vehicles (UCAV) and radar saturation roles.

There is a wide range of applications performed by UAVs in civil sphere, such as police [8], rescue [9] and firefighter needs [10], for example for traffic monitoring [11, 12], navigation [13, 14] and aerial mapping. UAVs are used for agriculture [15] needs, press, television, cinematography [16 – 18], marine application, pollution detection and other fields. They have generated great interest in industrial and academic areas [19, 20] due to small size, unique flight capacities [21, 22], outstanding maneuverability and low cost of mini UAV. Lot of research related to stability and controllability is being conducted [23 – 25].

Application areas lead to more advanced research for increasing the level of autonomy and reducing the size of UAVs. UAVs can be classified into two main categories: fixed-wing UAVs and rotary-wing UAVs. Fixed wing UAVs [26] constitute the richest group among these categories both in terms of research and utilization. They are able to fly for long duration at high speeds and their design is simple in comparison with the other types of UAVs. However, these UAVs suffer from the requirement of runways or additional launch and recovery equipment for takeoff and landing.

Rotary wing UAVs [27], on the other hand, are advantageous since they do not require any infrastructure for takeoff and landing. Neither do they need any forward airspeed for flight and maneuvering, which makes them useful

particularly in urban areas and indoors. This leads to a large variety of rotary wing UAVs.

Research and development of different UAVs is conducted in many universities around the world and well-known companies, like Bombardier Inc. and General Atomics. Unmanned aerial vehicle is a rapidly growing market with annual revenue of \$6.6 billion (in 2012) that will almost double over the next decade to \$11.4 billion (by Teal Group Corporation forecast) [28].

A wide variety of completely manufactured or sold in parts mini UAVs available are using standard power sources [29] whereas energy saving is a vital issue. Probable mini UAV is intended to obtain initial video information for police, rescuers and firefighter needs. For example, before sending a helicopter for extinguishing fire, firefighters would receive video information about the conflagrant areas and act more rationally and quickly. Unmanned aerial vehicles can assist rescuers in people search and help. Police can monitor large concentrations of people like at concerts and strikes to prevent incidents. The above applications and many others scopes of UAVs can save human lives and resources. It should be possible to carry the proposed UAV, for example, in a car. The mass of this vehicle should be 1.5 – 2 kg and size around 0.5 m (width and length).

### **Main objectives of the thesis**

The main aim is to decrease energy consumption of a multicopter. It is required to develop a methodology for the optimization of a multicopter by changing of the rotor placement and other geometrical parameters. To achieve this, it is necessary to investigate the methods of a multicopter design. Optimal distance between the rotors must be determined to reduce the consumption of energy by the motors and to maximize the lifting force created by the rotors, i.e. in this case mutual effect of air flows is minimal. Operation of propellers that have safety shrouds and coaxial rotor pairs must be analyzed for their energy consumption. It is required to find an optimal number of rotors to be used in a multicopter.

The objectives are as follows:

1. To develop a methodology for the optimization of the distance between the rotors in a multicopter for energy saving.
2. To find the dependence of the lifting force of the coaxial rotor pair on the changes of propeller sizes in pair.
3. To determine the influence of the clearance between the propeller and the shroud and the height of the shroud on the lifting force.
4. To find an optimal number of rotors in the multicopter.



The following steps are required to be taken:

- Verification of CFD (Computational Fluid Dynamics) simulation results by experiments. Firstly, propeller lifting force at different rotation speeds must be determined using software simulations. To acquire accurate results, real rotors need to be scanned with a 3D scanner and the models obtained used for all future analyses. Next, similar experiments with the same rotors must be conducted. It is necessary to build a force measurement device. During experiments it is required to measure propeller rotation speed and motor power consumption. The accuracy of CFD simulation results for mini UAV rotor calculations should be determined using the results obtained.
- Determination of the impact of rotor pitch on the lifting forces for different rotor diameters and different rotation speeds. Using the CFD calculations, results from different analyses of propellers with different diameters and pitches must be compared.
- Expediency of using coaxial rotor pairs in mini multicopters. Using already scanned propeller models, the lifting force of coaxial rotor pairs must be determined on different rotation speeds and compared with the lifting force of separately standing rotors. It is required to determine how the lifting force will change if propellers in pair are used with different diameters.
- Determination of the effect of protective frame around multicopter rotors on their lifting force and energy consumption. Using CFD simulations, it is necessary to compare the lifting force created by rotors with the force of fully opened rotors at the same rotation speed. It is required to verify the effect of dimensions (diameter and height) of the shroud around the rotor on the lifting force and the motor energy consumption.
- Comparison of energy consumption of multicopters with a different number of rotors. Mathematical energy consumption parameters of helicopters with 3, 4, 6 and 8 rotors need to be compared in hovering and horizontal flight.
- Impact of distance between quadrotor helicopter rotors on the lifting force and energy consumption. Using CFD simulations, quadrotor helicopters with different distances between rotors need to be compared. Simulations with different rotors diameters must be done. It is necessary to verify CFD simulations results with experiments.
- Methodology for the determination of an optimal distance between the rotors in the multicopter needs to be defined. The methodology should be suitable for UAVs with different masses, rotor diameters and their pitches.

## **ABBREVIATIONS**

CCW – Counter Clockwise

CFD – Computational Fluid Dynamics

CPU – Central Processing Unit

CNRS – Centre National de la Recherche Scientifique (National Center for Scientific Research)

CW – Clockwise

DC – Direct Current

ESC – Electronic Speed Controller

FVM – Finite Volume Method

LAAS – Laboratory of Analysis and Architecture of Systems

MARVIN – Multi-purpose Aerial Robot Vehicle with Intelligent Navigation

MAV – Micro Aerial Vehicle

MFI – Micromechanical Flying Insect

NACA – National Advisory Committee for Aeronautics

OIML – Organisation Internationale de Métrologie Légale (International Organization of Legal Metrology)

PC – Personal Computer

RC – Radio Control

RVP – Remotely Piloted Vehicle

SUAVI – Sabanci University Unmanned Aerial Vehicle

UART – Universal Asynchronous Receiver / Transmitter

UAV – Unmanned Aerial Vehicle

UCAV – Uninhabited Combat Aerial Vehicle

USB – Universal Serial Bus

VTOL – Vertical Take-Off and Landing

# 1. OVERVIEW OF THE LITERATURE

## 1.1 Flying types of mini UAVs

### Fixed wing UAV – plane

One of the most common aerial vehicles is a plane [30] – an aerodynamic aircraft for flights in the atmosphere by the engine and fixed wing. A plane is using the lift power of the wing to maintain itself in the air. It has some benefits for certain scopes, like ability to move at high speed on long distances. They are widely used for aero photo and video monitoring of long objects, like oil and gas trails or objects placed on long distances from a UAV launching place. Their disadvantages are that they cannot take off and land vertically (for those operations planes need fairly large spaces) and cannot hover in air. The flight characteristics of the plain are not very suitable for our tasks.

### Conventional helicopter

The most common type of a UAV is VTOL aircrafts (Vertical Take-Off and Landing), helicopter being one of them [31 – 34]. A helicopter – an aerodynamic aircraft is designed to take off and land vertically, hover in the air and move to any direction. Necessary lifting force and thrust are created by one or more rotors, driven by reciprocating or jet engines. The classical scheme of a helicopter: one large main rotor on top and a tail rotor to compensate the reactive moment. For mini UAVs this design has several disadvantages. It uses a mechanical swash plate for the flight control (with its help the angles of pitch and yaw can be changed) – so careful maintenance and in-time replacement are required. If something happens with the motor, energy supply, rotor or swash plate, such helicopter will fall. It is also possible to create a helicopter with two coaxial rotors where the tail rotor is not used.

One example of a conventional helicopter is Multi-purpose Aerial Robot Vehicle with Intelligent Navigation (MARVIN), Figure 1, designed by Technische Universität Berlin. MARVIN is an autonomously flying robot that can fulfill a complicated search mission purely on the basis of sensor data, without any human interaction [35].



*Figure 1. Helicopter MARVIN by Technische Universität Berlin [35].*

Furthermore, many different VTOL UAVs including helicopters from several designers such as the Guardian from Bombardier, and the Sikorsky's Cypher or Dragon Warrior can be operated in either wings-on or wings-off configurations. On the other hand, in recent years, Micro Air Vehicles with dimensions less than 15 cm have gained much attention. These include the Black Widow manufactured by AeroVironment, the MicroStar from BAE Systems and many new designs and concepts presented in several universities such as Entomopter (Georgia Institute of Technology), Micro Bat (California Institute of Technology), MFI (Berkeley University), as well as other designs in European Research Centers [1].

### Multi-rotor helicopters

A particular case of helicopters is a flying platform with 3 – 6 or 4 – 8 and more rotors. Helicopter (flying platform) with three rotors [36] like Tribelle from Braun Modelltechnik (Figure 2) that was awarded InterEx Unconventional Thinker Cup 2002 [37]. It has two rotors on each side of the fuselage, which rotate in opposite directions and the generated reaction torque is almost zero. The tail rotor can be tilted using a servomechanism in order to produce a yaw torque. The angular velocity of the two main rotors can be adjusted to produce the main thrust as well as the roll torque. The roll torque is obtained as a function of the angular speed difference of the two main rotors. Finally, the pitch torque is obtained by varying the angular speed of the tail rotor [38].

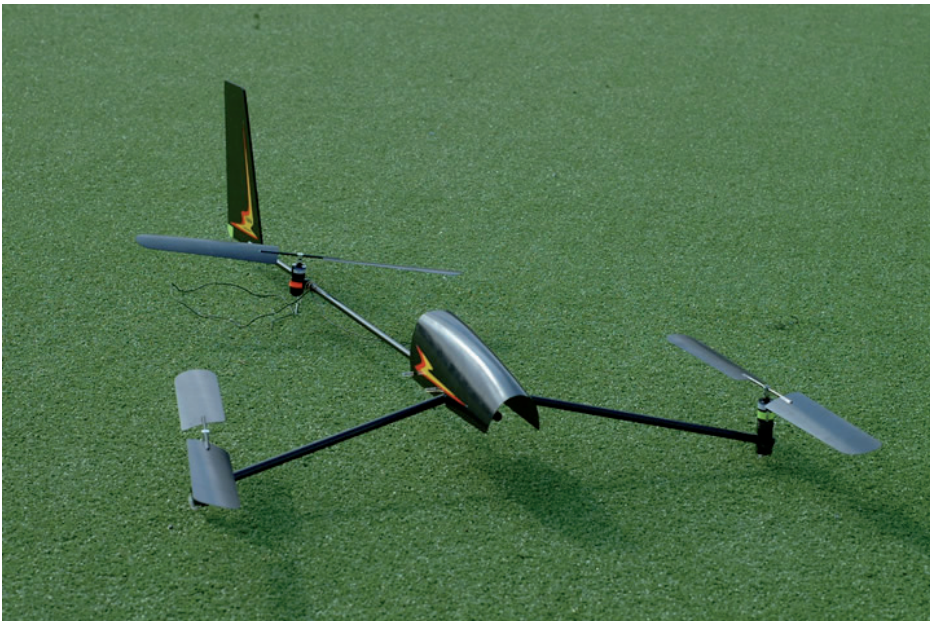


*Figure 2. Tricopter Tribelle, Braun Modelltechnik [37].*

Quadrotor (four rotor) helicopters, one of the most popular types of VTOL UAV platforms [39 – 41] (example in Figure 3), have several advantages over the traditional helicopters. These helicopters are more maneuverable and can turn around staying at one point. These vehicles use two pairs of counter-rotating, fixed-pitch rotors located at the four corners of the aircraft. These autonomous platforms are intended for a variety of applications, both as individual vehicles and multiple vehicle teams, including surveillance, search and rescue, and mobile sensor networks. They have two main advantages over the comparable vertical takeoff and landing UAVs. First, quadrotors can use fixed-pitch rotors and direct control of motor speeds, which help to simplify the design and maintenance by eliminating the complex mechanical control linkages for rotor actuation. Second, the use of four rotors ensures smaller individual rotors than the equivalent main rotor on a helicopter for a given airframe size. Smaller rotors store less kinetic energy during the flight and can be enclosed within a protective frame, permitting flights indoors and in obstacle-dense environments with reduced risk of damage to the vehicles, their operators, or surroundings. These added safety benefits greatly accelerate the design and test flight process by allowing testing to take place indoors or out, by inexperienced pilots, and with a short turnaround time for recovery from incidents [42].



*Figure 3. Quadcopter Draganflyer X4, Innovations Inc., picture from draganfly.com.*

Researches cover helicopters with six, eight and even twelve rotors which can hang more evenly in the air. Also, models with three or four pairs of coaxial rotors that rotate in opposite directions have been developed. This type of rotor location has some benefits in controllability but creates more noise.

## UAVs with other flying principles

The hybrid design of UAVs under consideration is the rotary-wing aircraft (tilt rotor or convertiplane) [43 – 45]. This aerodynamic aircraft is capable of vertical takeoff and landing (Figure 4) as it is a combination of a helicopter and a plane. It has both a wing and a rotor, like a helicopter, and a pulling propellers plane. Rotary-wing aircraft can make a vertical takeoff and landing, and the presence of wings with pulling propeller allows it to fly at a sufficiently high speed. Two significantly different modes of flight lead to many compromises in technical solutions and low efficiency of the aircraft. In another scheme of convertiplane, the propellers work as lifting rotors during take-off work, and turn around their transverse axis during the horizontal flight. This type of aerial vehicles has recently been actively developed in civil aviation and is becoming an attractive research area due to the stability, energy efficiency and controllability of the convertiplanes.

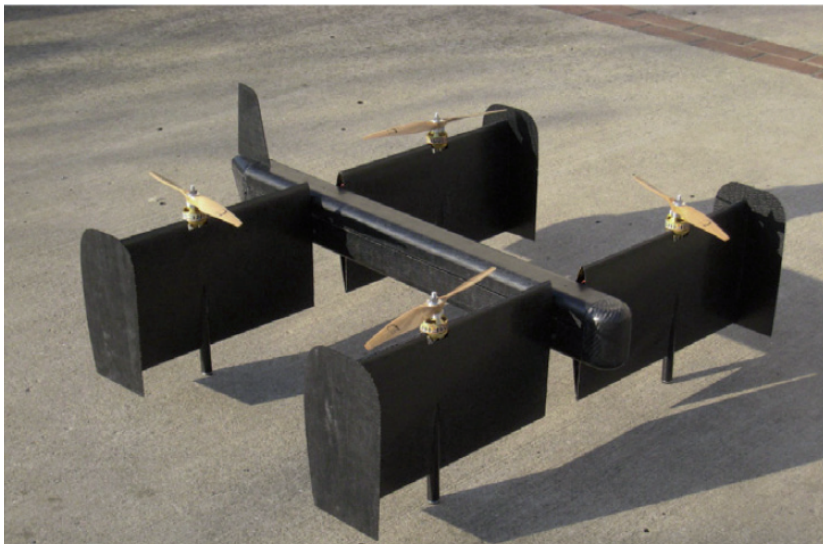


*Figure 4. Tilt rotor UAV SUAVI, Faculty of Engineering and Natural Sciences, Sabanci University, Orhanli-Tuzla, Istanbul, Turkey [43].*

Another more complex aerodynamical and mechanical design heavier than the normal aircrafts and still insufficiently studied is the flapping wings aircraft – ornithopter [46, 47]. Ornithopters have been developed for a long time. The first aerial vehicles would have to fly on the principle of birds. In recent years, thanks to the use of high-speed cameras it is possible to determine more accurately the trajectory of the wing movement of different birds and flying insects. Numerous working prototypes of ornithopters like a small toy UAV (Figure 5) from WowWee have been designed. Ornithopters have raised high interest because theoretically they could achieve a much higher efficiency than the aircraft that uses propellers or jet engines to create thrust.

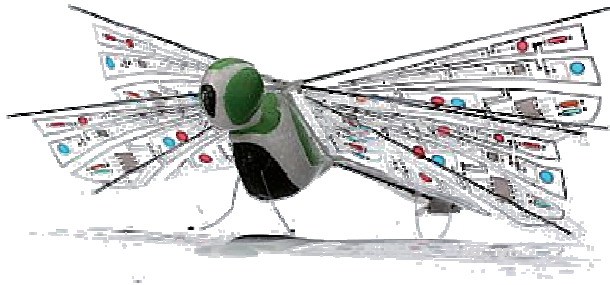


Figure 5. WowWee, ornithopter toy, picture from wowwee.com.

The lifting force and horizontal thrust of an ornithopter is created by the wing flaps, but not at the expense of air flow around an airfoil. The ornithopter can use a zero angle of attack and thereby greatly reduce the cost of energy to overcome air resistance. This type of aircraft is still insufficiently studied because of its complexity [47].

Another interesting type of VTOL aircraft is based on the Coanda effect [48]. This effect is a physical phenomenon which contains a stream of liquid or gas flowing from the nozzle that tends to deviate toward the wall and under certain conditions is adhering to it. With mini UAV, high pressure air is ejected from an annular slot on the top on the device (Figure 6) and flows around and down towards the bottom, entraining the surrounding air as it does so and creating a partial vacuum on the upper surface – a lower pressure region. Therefore, lifting force is produced [49, 50].

Separate regulation of airflows in different sectors by thruster "plates" allows it to bend and change course. This method of flight is a recent development and some UAVs based on this principle are available. For example, company AESIR released a model Vitar based on this method of flight with mass 400 g and flight duration of 15 min.

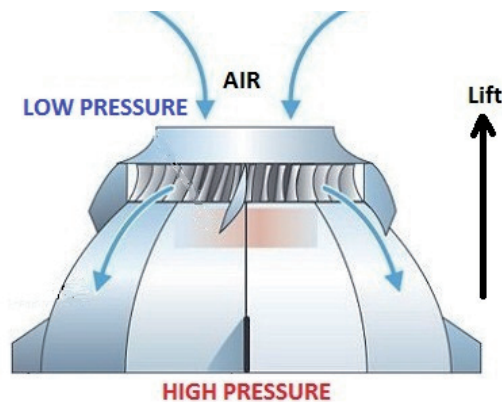


Figure 6. Scheme of UAV based Coanda effect, picture from flightglobal.com.

The world of UAVs offers more interesting unconventional flying prototypes, including airship Karma (Figure 7). Since many autonomous airplanes have been developed and used for reconnaissance, surveillance, environment monitoring and others tasks, airships in some areas can be more popular in the future than the other existing types of UAVs [1].



*Figure 7. Airship Karma, LAAS (CNRS, France) [1].*

Today two main goals of research prevail: to improve controllability and to increase energy saving. As long as there is no optimal aerial vehicle, new types will be developed, existing ones will be improved and optimized.



## 1.2 Optimization and energy saving of UAVs

Since today multicopters are very popular, intensive research work is conducted in this field, with focus on controllability and stability of flying platforms. In addition, interesting studies relate to energy saving of multicopters and their potentialities [51].

CFD calculation methodology is advancing. Special methods are being developed to calculate helicopter propeller blades like moving Overset Grids Method [52], where blade grids are cutting through an intermediate grid. Most of the studies are intended for large human operated helicopters but can be used also for mini UAVs. Thus, using the Single-Blade Based Hybrid CFD Method [53] with the concept of parallel computation, the CFD solver and rotor wake solver can be run independent of each other, and CPU time is reduced significantly. For a typical hover case, about 46.4 % of CPU time reduction can be achieved, while for a forward-flight case, more than 70 % of CPU time can be reduced, and the method is more efficient as the number of blades increases.

Optimized mini and Micro Aerial Vehicles (MAV's) rotors are also being developed by varying airfoil type, thickness, diameter, number of blades, and radial twist distribution [54], as shown in Figure 8. An interesting development of a constant chord propeller is presented in [55]. This type of a rotor that can be used in both manned and unmanned aerial vehicles has characteristics similar to those of usual rotors but it is cheaper in manufacturing.

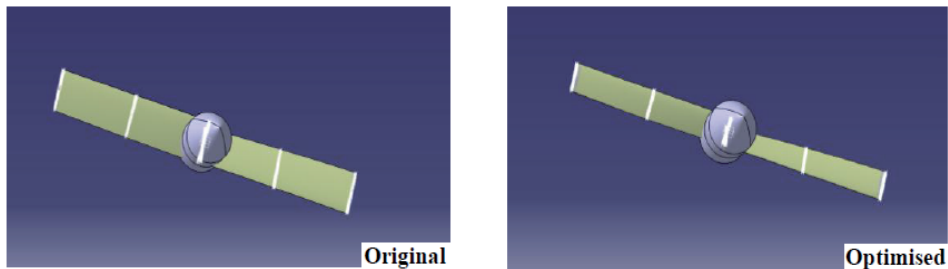


*Figure 8. Original and optimized rotor using CFD calculations of a MAV propeller [54].*

Since a rotor is working on the principle of a wing, they have similar problems in the tip of blades [56]. Vortexes that are created near the rotor ends lead to pressure adjustment between the upper and the lower rotor surfaces. Different studies cover the optimization of rotor blade tips [57]. Using an optimized rotor from the left of Figure 9, it is possible to reduce vorticity near rotating propeller blade ends, thereby reducing losses in the pressure difference near the upper and the lower rotor surfaces.

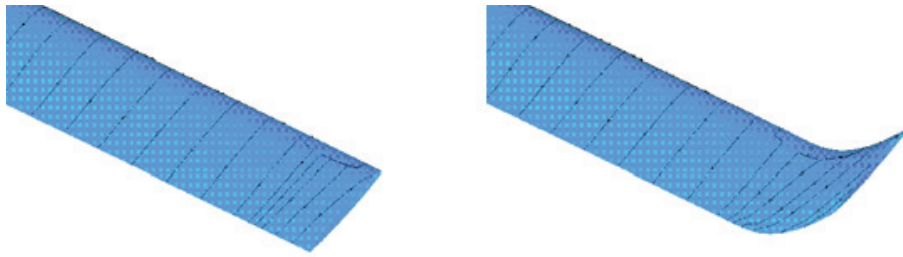


Figure 9. Helicopter rotor blade tip optimization [57]. Right – common rotor, left – optimized.

CFD simulations and experiment results made in the wind tunnels were also compared [58]. In other experiments for the determination of the thrust and the torque, self-made stands were used (Figure 10) [42, 59] where a load cell and a torque sensor are used for measurements. The data from the test stand were collected using an electronic data acquisition system. Results of those comparisons show the trustworthiness of different CFD software, indicating high accuracy of the results.

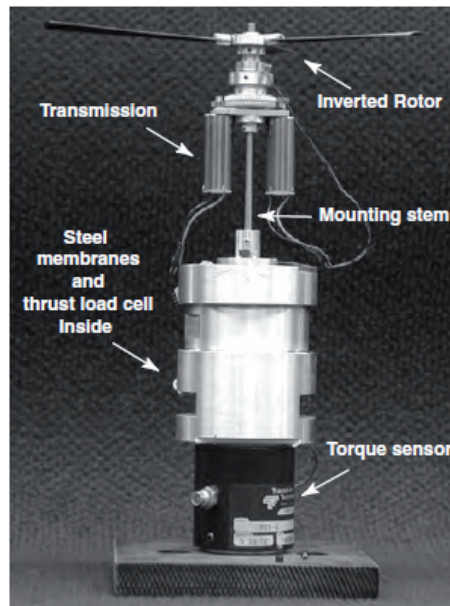


Figure 10. Stand for the determination of the lifting force and the torque [59].

Studies also cover coaxial rotors that rotate in opposite directions. Total lifting force of a coaxial rotor pair is usually 20 % lower than the force produced by two separately standing rotors [59].

In CFD simulations [60] made at Northwestern Polytechnical University (China), the distance between coaxial rotors was changed. It was found that by increasing the spacing between the two coaxial rotors, the thrust coefficient of

the top rotor increases, but the total thrust coefficient is slightly reduced because the decrease of the bottom rotor thrust coefficient is larger than the increase of the top rotor thrust coefficient. Optimization of the vertical distance between rotors ( $h$ ) and their radius ( $R$ ) shows that the  $h/R$  ratio is optimal between 0.41–0.65 for mini UAVs (Figure 11, in S.I. thrust is measured in Newton, but sometimes for simplicity of use thrust measured in grams) [61].

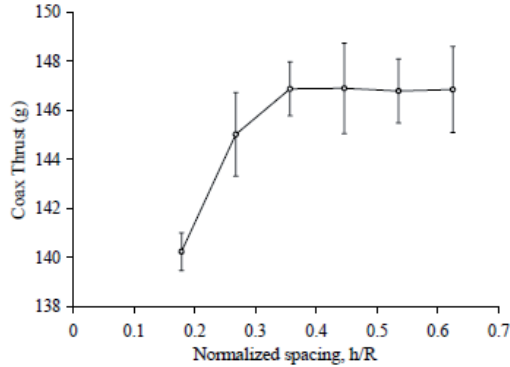


Figure 11. Dependence of the lifting force on rotor spacing in the coaxial rotor pair [59].

Many attempts have been made to create a shrouded rotor UAV. Most of them relate to ducted-fan UAVs with only one rotor (also called shrouded rotor). The reason is that according to the Rankine–Froude theory it can be more efficient than a usual helicopter with one fully opened rotor. Article [62] describes different geometrical changes of the duct, such as its diameter, height, propeller depth and cone angle (Figure 12). Change of the cone-angle of the duct may directly influence the airflow state at and near the inlet and outlet of the duct. Figure 12 (left) shows that the duct lift decreases gradually as the cone-angle increase from -6 degrees to 9 degrees. Thus, it confirms that a shroud is more efficient where the outlet is larger than the inlet.

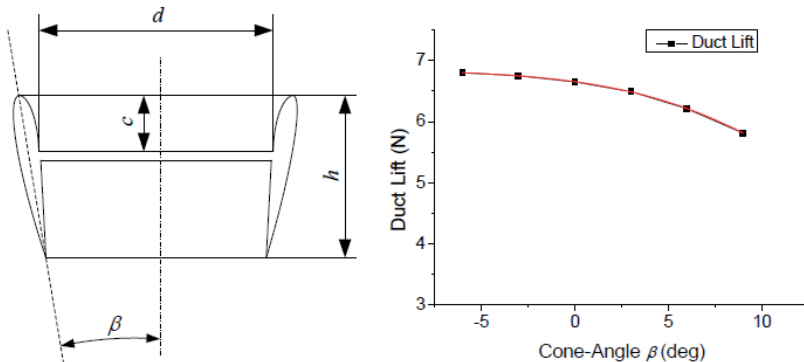


Figure 12. Analysis of the shroud cone angle [62].

A specific model of a shroud was calculated for use in the quadrocopter to increase the rotor's lifting force and to decrease energy consumption [63]. During the theoretical calculations, the efficiency was 167.5 % as compared to opened rotors. Unfortunately, those shrouds cannot be used in real life because of their weight.

A peculiar structure of a duct made at Harbin Institute of Technology contains four rotary cylinders symmetrically installed at the bottom of the inside duct [64]. Cylinders work on the Magnus effect, whereby a spinning object flying in a fluid creates a whirlpool of fluid around itself, and experiences a force perpendicular to the line of motion (Figure 13). The generated Magnus force can supply the control torque to stabilize the ducted-fan UAV, but not its lifting force.

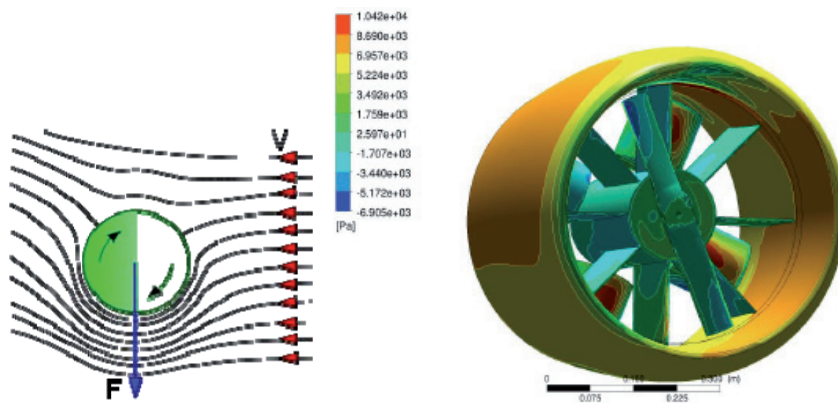


Figure 13. Left: Scheme of the Magnus effect, right: duct with four cylinders [64].

Aerodynamics of aerial vehicles is an area that needs further research and development of new ways of flight and optimization of existing ones to increase their flight characteristics and reduce energy consumption.

## 2. DETERMINATION OF ONE ROTOR LIFTING FORCE

### 2.1 Theory of propeller lifting force

Flight theory

A plane, a helicopter and other aerial vehicles are flying on the principle similar to lifting force creation. The body in the form of an airfoil (cross-section) or the blade (propeller, rotor or turbine) moving in the flow of gas or liquid creates a lifting force perpendicular to the direction of flow (Kutta–Joukowski theorem [65]). The lifting force (Figure 14 – lift), a component of the aerodynamic force [66], which is perpendicular to the velocity vector of the motion of the body in the flow of liquid or gas, occurs as a result of asymmetry of the streamline around the body.

In accordance with the law of Bernoulli, static pressure in the areas where the flow rate is higher will be lower and vice versa. This pressure difference pushes the wing up.

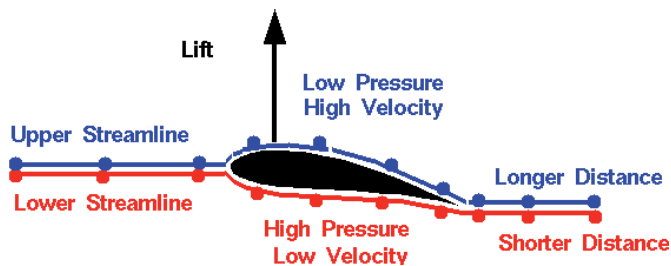


Figure 14. Origination of the lifting force of the body in the flow (this image is the property of NASA – free for non-commercial use).

The aerodynamic force for a plane can be expressed as follows [66]:

$$R = \int p \cdot n \cdot dA, \quad (1)$$

where

$R$  – aerodynamic force,

$p$  – value of the pressure,

$n$  – normal unit vector pointing into the wing,

$A$  – wing surface area.

The same force for a helicopter can be shown as [66]:

$$R = \pi \frac{D^2}{4} V \rho u, \quad (2)$$

where

$D$  – diameter of the rotor,

$V$  – flight speed,

$\rho$  – density of air,

$u$  – induced velocity of the outgoing stream.

### Theory of propeller lifting force

Rotors for aerial vehicles are also called aircraft propellers or airscrews (for helicopters and multicopters, rotor is the common name). They convert rotary motion from engine to provide propulsive force. Propeller blades are designed using airfoil sections to produce an aerodynamic force, in a similar manner to a wing. Propellers can be classified by the number of blades (one, two, three, four and more), by the location relative to the motor (pulling and pushing), by the shape of blades, pitch (fixed and variable pitch) and some other parameters [67].

Propeller pitch is defined as the distance a propeller would move in one revolution if it were moving through a soft solid, like a screw through wood. For example, a 127 mm (5 in) pitch propeller would move forward 127 mm in one revolution. Each point of the propeller, from the hub to the blade tips, has the same forward velocity, the rotational velocity – and thus the helical path of any blade station – will depend on its distance from the rotation axis [68]. The blade angle is the angle that the chord line of the airfoil makes with the propeller's rotational plane ( $\varphi$  in Figure 15) and this angle follows from the pitch. Because of the twist, the blade angle will vary throughout its length. So, normally the standard blade angle is measured at the blade station 75 % of the distance from the hub center to the blade tip [69].  $\alpha$  in Figure 15 shows the angle of attack that corresponds to the angle between the cord line and the real rotor movement. Propellers operate most efficiently when the angle of attack at each blade station is consistent over most of the blade, so a twist is built into the blades to achieve a more or less uniform attack angle [70]. Pitch is fixed usually to 30 – 70 % of the propeller diameter.

In mini aerial vehicles and multicopters propellers with two blades and fixed pitch are used. Pitch is fixed usually to 30 – 70 % of the propeller diameter.

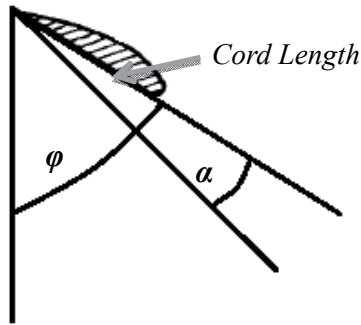


Figure 15. Propeller blade angle ( $\varphi$ ) and angle of attack ( $\alpha$ ).

### CFD simulation

Computational fluid dynamics, usually abbreviated as CFD, is a branch of fluid mechanics that uses numerical methods and algorithms to solve and analyze problems that involve fluid flows. Flow simulations on computer were made with CFD software SolidWorks Flow Simulation (versions 2010 – 2013).

Rotary-wing vehicles encounter a wide variety of complex aerodynamic phenomena and these phenomena present substantial challenges for CFD models [71]. In the 1970s, computational fluid dynamics technology was first applied to the rotorcraft research and significant improvements were achieved during the past several decades. There are mainly two methodologies used for wake computation in the rotor CFD analysis. First, the so-called Eulerian method, which models the whole rotor system and attempts to capture the wake structure entirely from the first principles. This approach was initiated in the 1980s for hovering rotors [53, 57]. Second, Navier–Stokes equations are used throughout the blade grid [72]. Although the Navier–Stokes solvers can capture strong shock wave and predict air-loadings well, their use in the region outside the boundary layer is costly because the flow is irrotational and viscous effect is negligible.

Flow Simulation solves the Navier–Stokes equations, which are formulations of mass, momentum and energy conservation laws for fluid flows. The equations are supplemented by fluid state equations defining the nature of the fluid, and by empirical dependencies of fluid density, viscosity and thermal conductivity on temperature [73]. The derivation of the Navier–Stokes [74] equations begins with an application of Newton's second law: conservation of momentum (often alongside mass and energy conservation) being written for an arbitrary portion of the fluid. In an inertial frame of reference, the general form of the equations of fluid motion is the Navier–Stokes Eq. (3) [75, 76]:

$$\rho\left(\frac{\partial \mathbf{v}}{\partial t} + \mathbf{v} \cdot \nabla \mathbf{v}\right) = -\nabla p + \nabla \cdot \mathbf{T} + \mathbf{f}, \quad (3)$$

where

$\mathbf{v}$  – flow velocity,

$\rho$  – fluid density,

$p$  – pressure,

$\mathbf{T}$  – viscous part of stress tensor,

$\mathbf{f}$  – represents body forces acting on the fluid,

$\nabla$  – del operator.

This equation is often written using the material derivative  $D\mathbf{v}/Dt$ , Eq. (4), making it more apparent that this is a statement of Newton's second law [76].

$$\rho \frac{D\mathbf{v}}{Dt} = -\nabla p + \nabla \cdot \mathbf{T} + \mathbf{f}. \quad (4)$$

The left side of Eq. (4) describes acceleration, and may be composed of time dependent or convective effects (also the effects of non-inertial coordinates if present). The right side of the equation is in effect a summation of body forces (such as gravity) and divergence of stress (pressure and shear stress).

The finite volume method (FVM) is a common approach used in CFD codes. The governing equations are solved over discrete control volumes. Finite volume methods recast the governing partial differential equations (Navier–Stokes or Euler equations [52]) in a conservative form, and then discretize the new equation. This guarantees the conservation of fluxes through a particular control volume. The finite volume equation yields governing equations in the form Eq. (5) [73]:

$$\frac{\partial}{\partial t} \iiint Q \cdot dV + \iint F \cdot dA = 0, \quad (5)$$

where

$Q$  – vector of conserved variables,

$F$  – vector of fluxes,

$V$  – volume of the control volume element,

$A$  – surface area of the control volume element.



Flow Simulation is capable of predicting both laminar and turbulent flows. Laminar flows occur at low values of the Reynolds number ( $Re$ , a dimensionless number that gives a measure of the ratio of inertial forces to viscous forces and consequently quantifies the relative importance of these two types of forces for given flow conditions), which is defined as the product of representative scales of velocity and length divided by the kinematic viscosity. When the Reynolds number exceeds a certain critical value, the flow becomes turbulent, i.e. flow parameters start to fluctuate randomly. Moreover, transition from a laminar to a turbulent state and/or vice versa is possible [73].

Any SolidWorks Flow Simulation calculation is performed in a rectangular parallelepiped-shaped computational domain the boundaries of which are orthogonal to the axes of the global coordinate system. A computational mesh splits the computational domain with a set of planes orthogonal to the coordinate system's axes to form rectangular parallelepipeds called cells. The resulting computational mesh consists of cells of different types. Fluid cells are the cells located entirely in the fluid, solid cells are located entirely in the solid and partial cells are the cells which are partly in the solid and partly in the fluid. Also, cells can be divided onto triangles. The curvature refinement level is the maximum level to which the cells will be split during refinement of the computational mesh until the curvature of the solid/fluid or fluid/porous interface within the cell becomes lower than the specified curvature criterion. Firstly, each solid surface is triangulated: software obtains triangles that make up surfaces. Secondly, a local (for each cell) interface curvature is determined as the maximum angle between the normals to the triangles within the cell. Thirdly, if this angle exceeds the specified curvature criterion and the curvature refinement level is not reached, then the cell is split [73].

## 2.2 Lift force determination

### Simulations

Simulations for the determination of the lifting force were conducted with SolidWorks Flow Simulation. The real rotors (DF-1050CR from Draganfly Innovations, airfoil type similar to NACA6409) were previously scanned with a 3D scanner, then imported in SolidWorks as point cloud data and working models were created (Figure 16). After this rotor lifting force was determined at different rotation speeds.

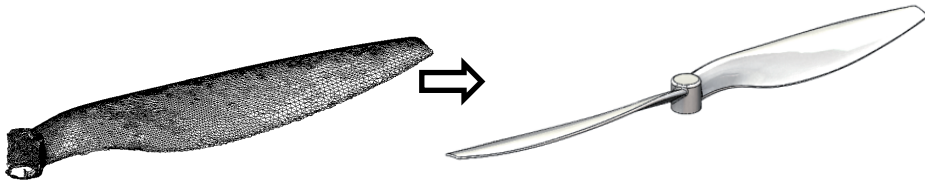


Figure 16. Models for CFD simulation created using 3D scanned data.

CFD simulations were made using external computational domain with a local rotating region. This option is employed to calculate flows in the regions surrounding rotating non-axisymmetrical solids like impellers, mixers, propellers, etc. Environment is filled by air with a molecular mass of 0.02896 kg/mol. Normal environmental conditions with pressure 101325 Pa and temperature 20 °C are used. Temperature change effects are not taken into account. Meshing is done using manual mesh control using planes and mesh refinement around rotor's curved surfaces (Figure 17). Mesh refinement reduces the number of partial cells (cells that are partly in the solid and partly in the fluid). All the simulations made in steady-state mode until convergence of the lifting force will be less than 0.02 N (around 0.3 % of the whole amount of the lifting force).

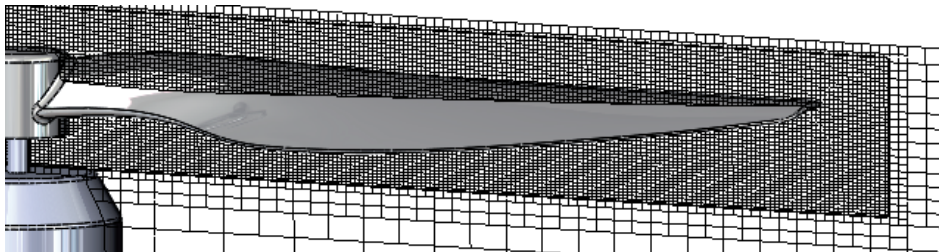


Figure 17. FVM mesh for 254 mm (10 in) rotor simulation.

In Figure 18, streamlines and vectors show air velocity and direction of flow. Colors show pressure difference near the rotating rotor. Pressure difference between the top and bottom surfaces of the rotor creates the lifting force, Eq. (1). Rotating rotor ends create a turbulent area, where the flow goes upwards and this stream partially compensates lower pressure region on top and the lifting force decreases.

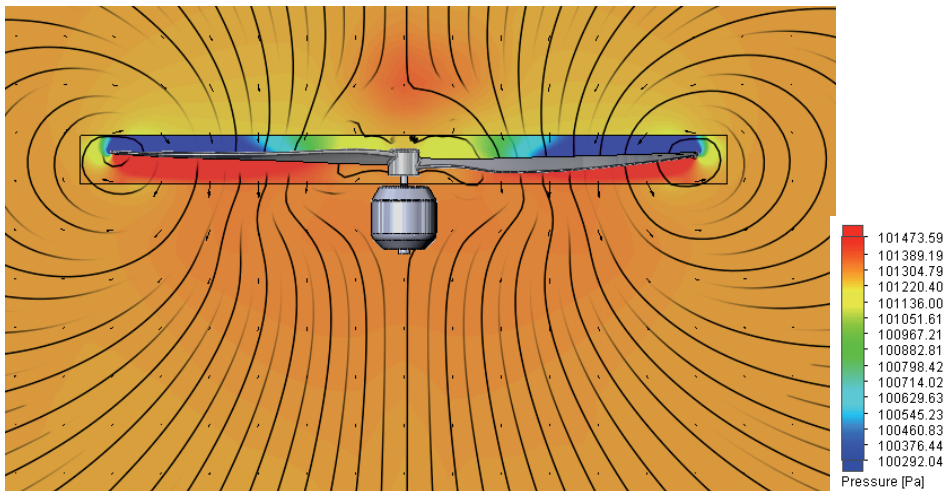


Figure 18. CFD simulation of 254 mm (10 in) rotor. Streamlines and vectors show air velocity, colors show pressure.

### Testing device

In experiments a brushless motor Robbie 2827-34 with rotors 254 x 127 mm and 203.2 x 101.6 mm (10 x 5 in and 8 x 4 in) were used. For motor control a brushless motor controller (ESC) BL-CTRL 1.2 from the Mikrokopter company was used, operated through RS232 port directly from PC (using UM232R USB Serial UART Development Module by FTDI company). For control, freeware software KopterTool V1-78B from a brushless motor controller developer was used. To determine motor power consumption a bypass resistor was used. Experiments were built by a testing device in Figure 19. Heavy base is fixed with a strain gauge sensor PS-08844244 with a motor with a rotor fixed to it. Rotor rotation speed was measured with an optical laser tachometer Omron CT6. Altogether 10 rotor's rotational speed was measured for each rotor size.

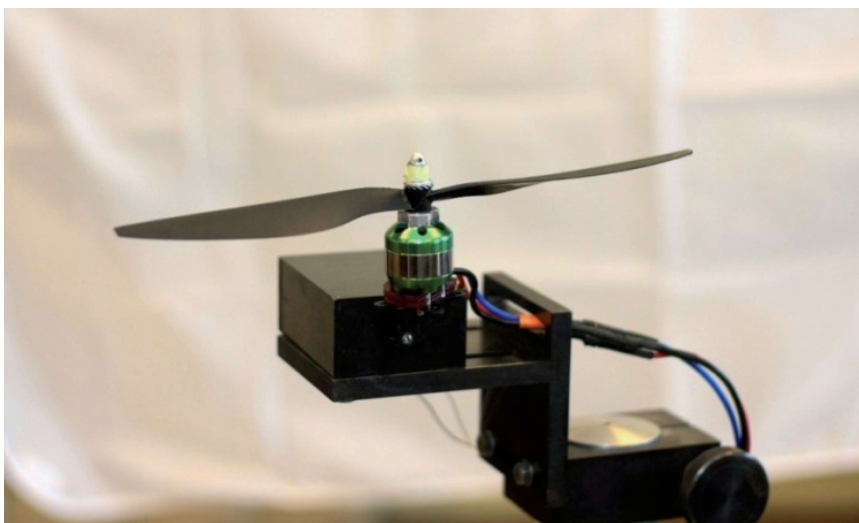


Figure 19. Testing device for the determination of rotor lifting force.

A previously calibrated strain gauge sensor was used for force determination. It consists of a pattern of resistive foil mounted on a backing material. Its principle of operation is: as the foil is subjected to stress, the resistance of the foil changes in a defined way. The strain gauge is connected into a Wheatstone bridge circuit with a combination of four active gauges (full bridge). The complete Wheatstone bridge is excited with a stabilized DC supply. As stress is applied to the bonded strain gauge, resistive changes take place that unbalance the Wheatstone bridge [77]. Figure 20 shows the electric scheme of the connection.

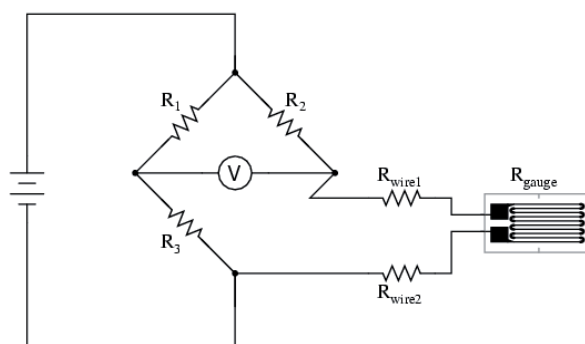


Figure 20. Electric scheme of the connection of a strain gauge sensor to the Wheatstone bridge resistors scheme, picture from [www.allaboutcircuits.com](http://www.allaboutcircuits.com).

For strain gauge sensor calibration laboratory weights (OIML M<sub>1</sub> class) were used. They were applied to the rotation axis of the rotor. Since the sensor has linear dependency (Figure 21, nonlinearity  $\pm 0.7\%$ ), it is possible to describe its behavior by Eq. (6).

$$F = 71.72 \cdot V + 1.02, \tag{6}$$

where

$F$  – load applied to the sensor, N,

$V$  – voltage measured on the sensor, V,

and the coefficients with units are 71.72 N/V and 1.02 N.

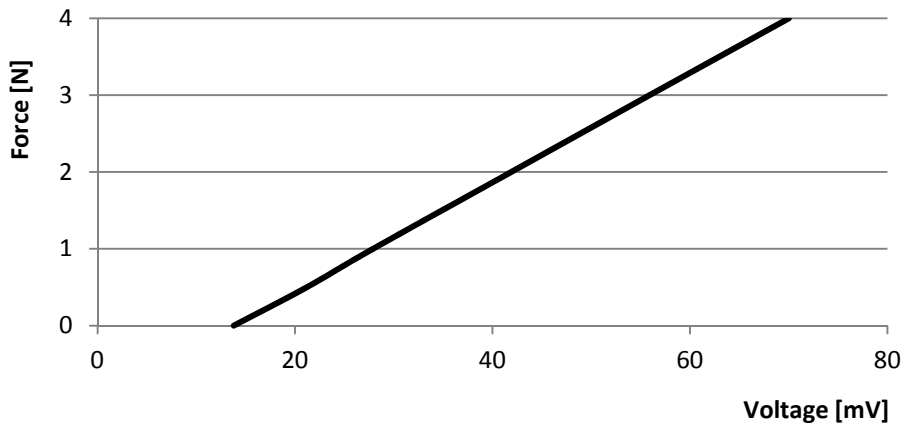


Figure 21. Results from the experiment with voltage measurements on the strain gauge sensor with different loads.

## Experiments

Experiments were done on the testing device with two different rotors 254 x 127 mm and 203.2 x 101.6 mm (10 x 5 in and 8 x 4 in). Both rotor size experiments were repeated three times. With the signal strength changing the rotor rotation speed and the measured lifting force produced by the rotor, motor power consumption, and real rotation speed changed.

With rotation speed increase the velocity of air flow near upper and lower rotor blade surfaces increases. Since upper rotor surface have bigger surface area, flow velocity increases there more than near lower rotor surface. According to Bernoulli law pressure difference near lower and upper surfaces increases. This pressure difference creates force (according to Eq. (1)) directed upwards and it increases with augmentation of rotor rotation speed.

Experiment results were approximated using non-linear regression analysis in Microsoft Excel software. Lifting force dependency on the rotor rotation speed can be expressed in Eq. (7), coefficient of determination  $R^2 = 0.98$ . The data of the experiment and the approximated curve are presented on one graph in Figure 22.

$$F = 0.486 \cdot 10^{-6} \cdot n^{1.882}, \quad (7)$$

where

$n$  – rotor rotation velocity,  $\text{min}^{-1}$ ,

$F$  – produced lifting force, N,

and the coefficient with units is  $0.486 \cdot 10^{-6} \text{ N} \cdot \text{min}^{1.882}$ .

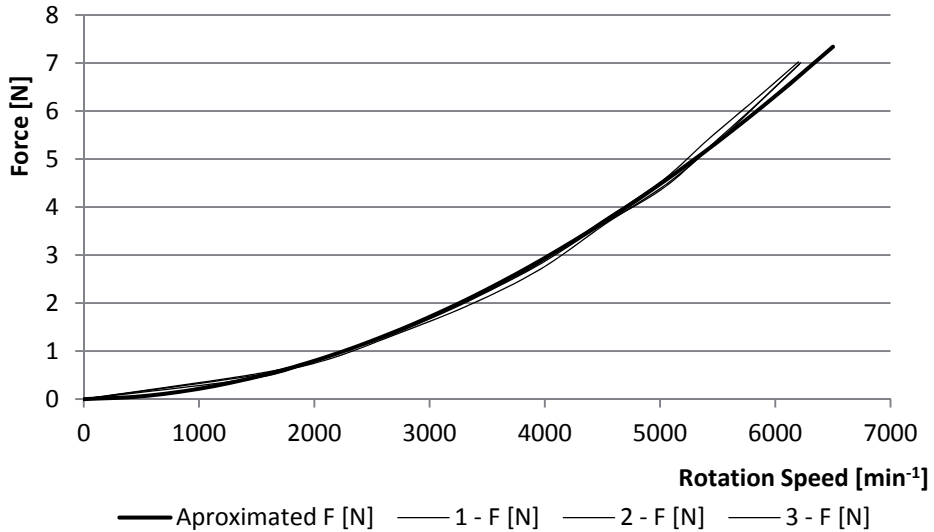


Figure 22. Data of three experiments and approximated result of the dependency of the lifting force on the rotation speed, 254 mm (10 in) rotor.

### Power consumption measurement

Power consumption was measured with a bypass resistor SH-15-30A-75 with voltage 75 mV and current 15/30 A. Power consumption during the experiment with 254 mm (10 in) rotor is shown in Figure 23. Each step on the graph corresponds to a certain rotor rotation speed and energy consumption in hovering is stable. Figure 24 shows the dependency of the lifting force on motor power consumption (approximated results).

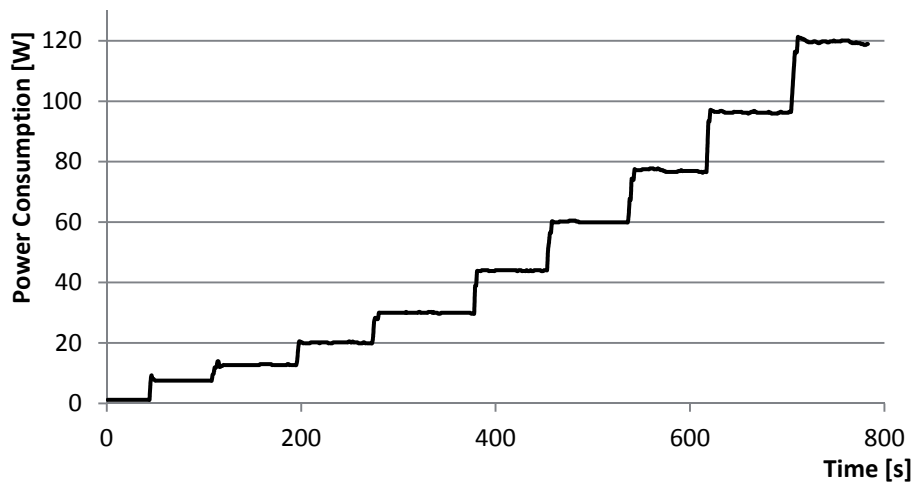


Figure 23. Motor power consumption in time.

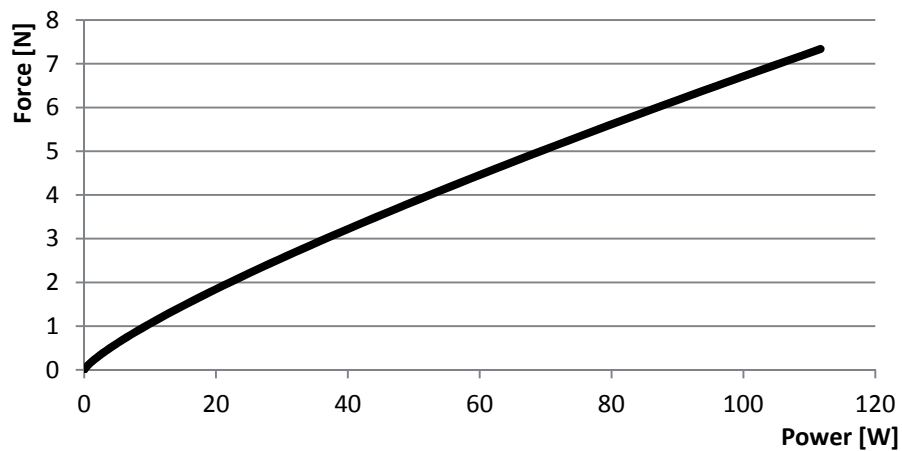


Figure 24. Dependency of the lifting force on motor power consumption.

Motor power consumption behavior can be described as linear ( $R^2 = 0.99$ ) at least at working angular velocities (when rotor creates 0.5 N – 7 N of lifting force). Also, rotation speed on power consumption dependency is close to linear in our case. Usually motor energy consumption on the dependence of rotation speed has a paraboloid form, where at lower rotation velocity power consumption is proportionally lower than at higher velocities. The goal is to achieve the least propeller rotation speed to create the same amount of the lifting force.

### 2.3 Comparison of simulation and experiment results

Figure 25 illustrates force dependency on the rotor rotation speed, left graph compares forces produced by 254 mm (10 in) rotor and right graph shows the same data for 203.2 mm (8 in) rotors. An experiment force graphs were created with the experiment data ( $R^2 = 0.99$ ) and CFD force graph with simulation.

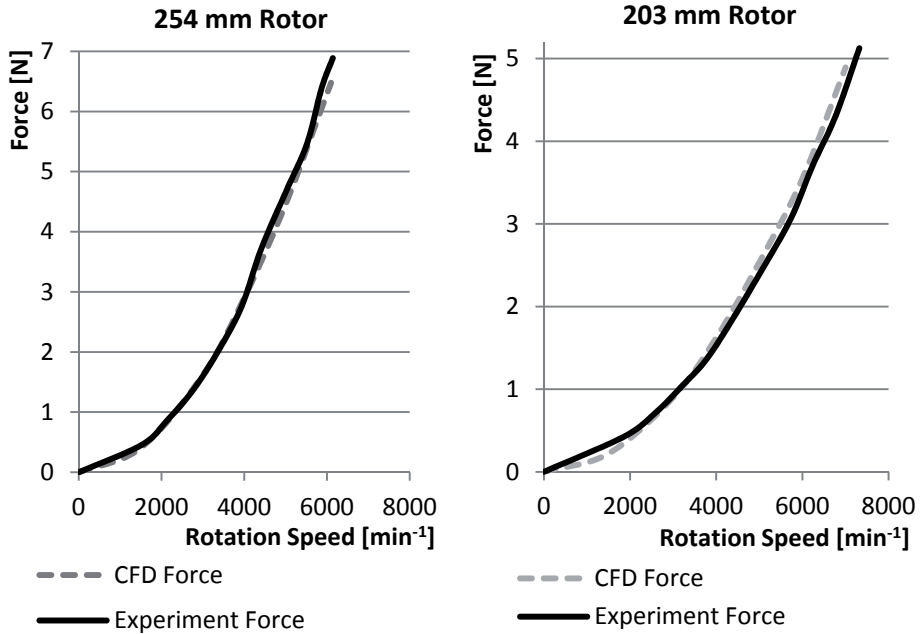


Figure 25. Dependency of the lifting force on the rotation speed for 254 and 203 mm (10 in) rotors.

Both methods give approximately similar results (maximum difference is 3.32 %). This means that we can use CFD software for similar future analysis and calculation of the impact of flows from different rotors on each other.



## 2.4 Rotor pitch calculation

### Rotor pitch

Air propellers that are available on the market have different pitches (described in section 2.1). Theoretically, the higher the pitch, the higher lifting force can be produced. In real life an increase in pitch size will create an additional load on the motor and its combination with the rotor may be ineffective. The best way to choose the right size of the rotor is to follow the motor manufacturer's recommendations [78, 79]. Usually pitch changes in the range of 0.3 – 0.7 of the diameter of the rotor. Median value of pitch is half of a rotor's diameter. All the other simulations use rotors that have pitch equal to half of the diameter.

### Simulations

Simulations will compare rotors with the same diameter and rotating at the same rotation velocity but with different pitches. As a point on the rotor blade travels around in a circle, it advances according to pitch, the angle of the blade, at a distance from the hub with a given pitch can be found by Eq. (8). For example, Figure 26 shows 254 mm (10 in) rotors with pitch 76.2 mm, 101.6 mm, 127 mm and 152.4 mm (3, 4, 5 and 6 inches respectively). Angles between the rotor cord and the horizontal plane are 5.46 deg, 7.26 deg, 9.04 deg and 10.84 deg, respectively.

$$P = \tan \alpha \cdot 2\pi R,$$
$$\alpha = \arctan \cdot \left( \frac{P}{2\pi R} \right), \quad (8)$$

where

$\alpha$  – angle between the rotor cord and the horizontal plane, deg,

$P$  – rotor pitch, mm,

$R$  – rotor diameter, mm.



Figure 26. 254 mm (10 in) rotors with pitches 76.2 mm, 101.6 mm, 127mm and 152.4 mm (3, 4, 5 and 6 inches respectively).

To find how the rotor pitch affects the lifting force, simulations were made with the use of CFD software. Firstly, simulations were made for a rotor with a length of 254 mm (10 in). Figure 27 shows the dependency of the lifting force

on the rotor pitch for different rotation speed. Those dependencies can be described as linear with a high coefficient of determination. Simulations were made only on “working” rotor rotation speeds that can be used in real life ( $2000 \text{ min}^{-1} - 8000 \text{ min}^{-1}$ ).

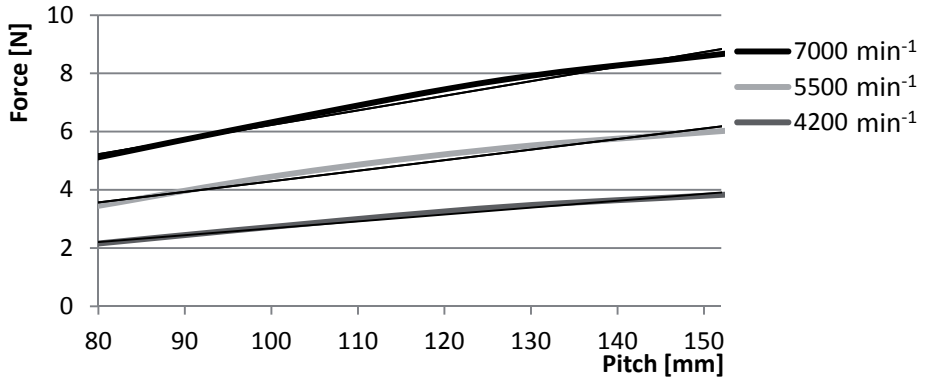


Figure 27. Dependency of the lifting force on pitch for 254 mm (10 in) rotor.

Combining all three dependencies will get relation how the lifting force depends on the rotor pitch. Pitch correction for 254 mm (10 in) rotor can be expressed by Eq. (9),  $R^2 = 0.98$ .  $F_{C-10}$  can take both positive and negative values, depending on the pitch higher or lower than 127 mm (5 in). Adding parameter  $F_{C-10}$  to the lifting force will show how the lifting force will change if a pitch different from 127 mm (5 in) is used. This equation is not related to the rotation speed (and therefore unrelated to the exact lifting force).

$$F_{C-10} = (P - 127) \cdot 0.037, \quad (9)$$

where

$F_{C-10}$  – 254 mm (10 in) rotor pitch correction, N,

$P$  – pitch, mm,

and the coefficients with units are 127 mm and 0.037 N/mm.

Simulations for the determination of the dependency of the lifting force on pitch were also made for 203.2 mm and 304.8 mm (8 in and 12 in) rotors. Those dependencies are also linear and can be described by Eqs. (10), similar to Eq. (11).

$$\begin{aligned} F_{C-8} &= (P - 101.6) \cdot 0.018, \\ F_{C-12} &= (P - 152.4) \cdot 0.051. \end{aligned} \quad (10)$$

Combination of Eqs. (9) and (10) will results in the overall pitch correction coefficient  $F_C$  (Eq. (11) with  $R^2 = 0.94$ ). Using the parameter  $F_C$  it is possible to forecast how the lifting force will change if the pitch different from half of the diameter is used. This formula will work reliably when pitch is 0.3 – 0.7 of the diameter of the rotor at rotor rotation velocities  $2000 \text{ min}^{-1} - 8000 \text{ min}^{-1}$ .

$$F_C = \left( P - \frac{D}{2} \right) \cdot \left( 3.27 \cdot 10^{-4} \cdot D - 4.72 \cdot 10^{-2} \right), \quad (11)$$

where

$F_C$  – pitch correction, N,

$P$  – pitch, mm,

$D$  – rotor diameter, mm,

and the coefficients with units are  $3.27 \cdot 10^{-4} \text{ N/mm}^2$  and  $4.72 \cdot 10^{-2} \text{ N/mm}$ .

### 3. FINDING OPTIMAL WAY OF ROTOR USAGE

#### 3.1 Coaxial rotors

Multicopters with coaxial rotors

Mini UAV helicopters can be designed with one rotor on the axis and with two coaxial rotors (Figure 28) [60]. A rotating rotor in a helicopter creates an angular momentum that rotates the helicopter around. In a usual quadrotor helicopter (with a single rotor on the axis) angular momentum is compensated by the rotation of the rotor pairs in the opposite direction. In helicopters with two rotors that are located on the same axis and rotated in different directions torques created by rotors compensate each other. In this case three pairs of coaxial rotors – a tricopter without any compensating or sloping mechanism can be used. In order to ensure the lifting force directed upwards, upper and lower rotors have opposite versions. One rotor rotates clockwise (CW) and the other rotates counter clockwise (CCW).



Figure 28. Draganflyer X6 with three pairs of coaxial rotors, Innovations Inc., picture from draganfly.com.

Theory of coaxial rotors

Moment of inertia ( $J$ ) can be obtained by considering the rotational motion of a mass of the body ( $B$ ) [80]:

$$J = \int_B r^2 dm, \tag{12}$$

where

$r$  – radial distance of the mass elements  $dm$  from the axis,

$m$  – mass of the body.

For simplicity, considering the rotating rotor to be a symmetric rod (actually its cross-section is not constant) that rotates around its own symmetry axis. Its moment of inertia can be described as Eq. (13).

$$J = \frac{1}{12} m \cdot l^2, \quad (13)$$

where

$l$  – length of the rod.

Angular momentum ( $L$ ) of a rotating body around axes can be calculated using Eq. (14) [80].

$$L = J \cdot \omega, \quad (14)$$

where

$\omega$  – angular velocity.

The angular momentum (Eq. (15)) of a symmetric rod can be presented by combining Eqs. (13) and (14).

$$L = \frac{1}{12} m \cdot l^2 \cdot \omega, \quad (15)$$

where

$m$  – mass of the body,

$l$  – length of the rod,

$\omega$  – angular velocity.

In Figure 29  $m_u, l_u, \omega_u$  corresponds to mass, length and angular velocity of the upper rotor and  $m_l, l_l, \omega_l$  to the lower rotor, respectively. If in coaxial pair are used two identical rotors with same angular velocity ( $m_u = m_l, l_u = l_l, \omega_u = \omega_l$ ), then  $L_u = L_l$ . Angular momentums compensate each other as far as rotors rotate in opposite directions [81].

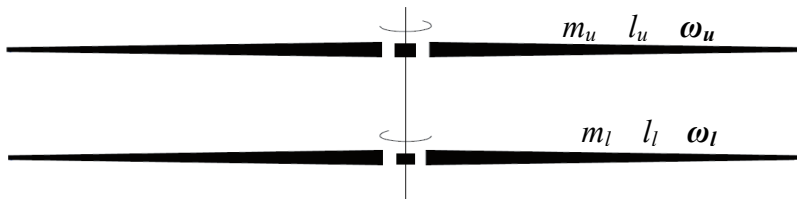


Figure 29. Two coaxial rotors with the same diameter [81].

In another case of coaxial rotors layout, upper and lower rotors with different dimensions are used [81]. In this case  $m_u \neq m_l$  and  $l_u \neq l_l$ . For angular momentum compensation ( $L_u = L_l$ ) both rotors must rotate at different angular velocities ( $\omega$ ). Simulation results presented below describe the upper and lower rotors having the same angular velocity in all cases.

### Simulations

In the first series of CFD simulations two coaxial 254 mm (10 in) rotors are used and the force produced at different rotation speeds is determined. Combined lifting force created by a pair of coaxial rotors is less than the lifting force created by two separately standing rotors of the same size. Graph in Figure 30 compares forces produced by two coaxial 254 mm (10 in) and one separately standing rotor. For example, one 254 mm (10 in) rotor produce 4.46 N lifting force at the rotation speed of  $5000 \text{ min}^{-1}$ . Two coaxial rotors are creating 7.03 N of force at the same velocity. This lifting force is 21 % lower than the force created by two separately standing rotors in the same size.

The upper rotor creates an air velocity directed on the lower one and the flow is twisted in the opposite direction, as compared to the lower rotor. Air velocity from the upper partially compensates pressure difference near the lower rotor (Figure 31). Therefore, the lifting force created by the lower rotor will be decreased. When using two 254 mm (10 in) rotors, the lifting force created by the upper is around 70 % of the whole rotor pair force. The lower rotor creates only 30 % of the full lifting force (Figure 32).

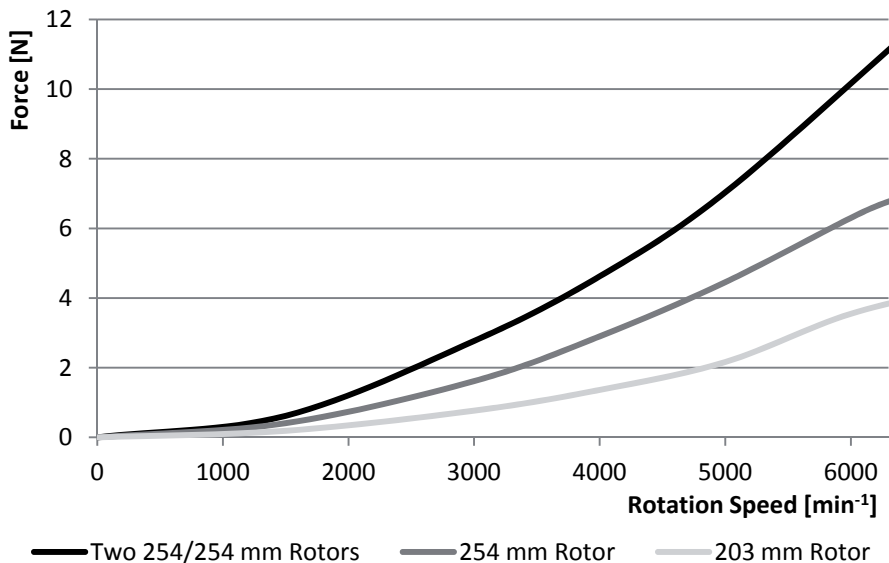


Figure 30. Comparison of the lifting force produced by two coaxial 254 mm (10 in) rotors and separately standing rotors 254 mm and 203 mm (10 in and 8 in).

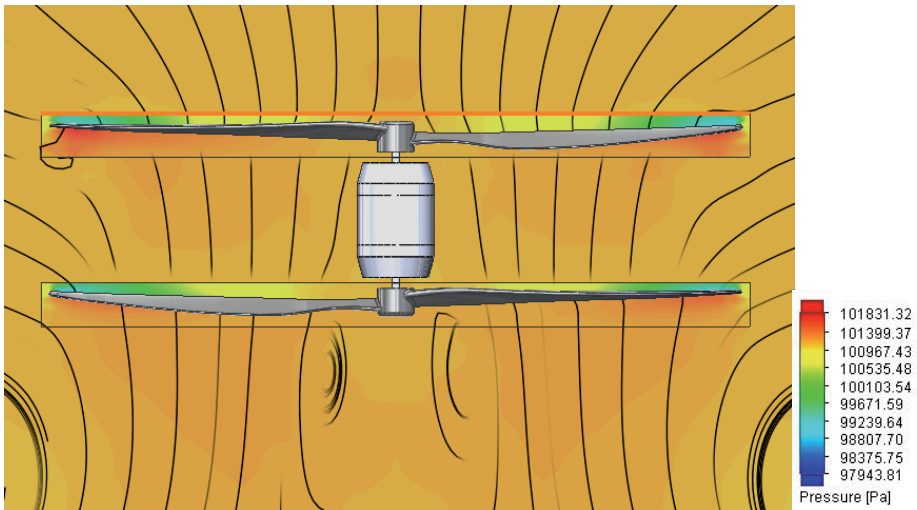


Figure 31. Pressure distribution near two rotating coaxial rotors of the same size, 254 mm (10 in).

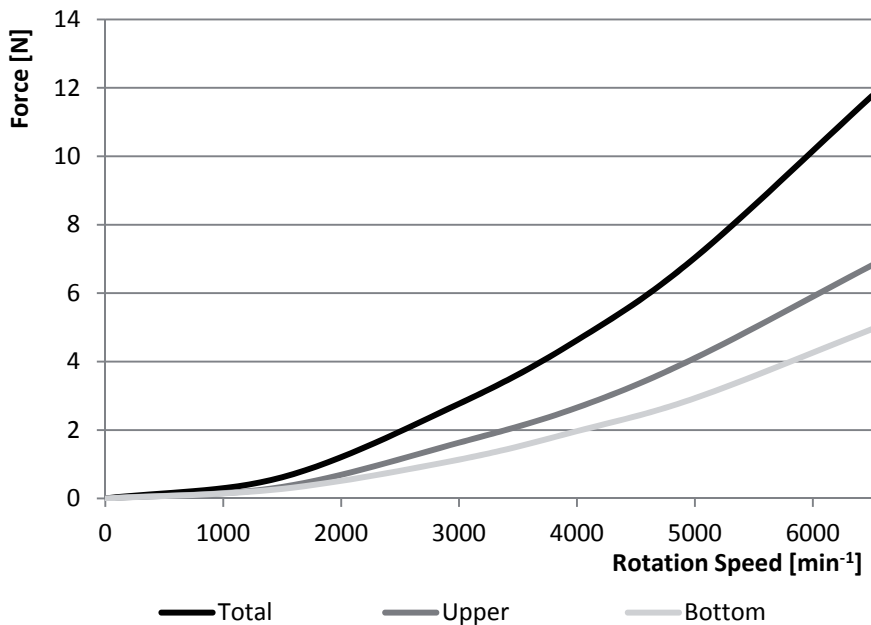


Figure 32. Lifting forces created by lower and upper rotors in the coaxial rotor pair, 254 mm (10 in).

Next, pairs of coaxial rotors with different rotor sizes in pair will be compared. The first pair has a large 254 mm (10 in) rotor on top and a small 203 mm (8 in) one in the bottom that are rotating in opposite directions (left side of Figure 33). The second pair of rotors is located vice versa (right side of Figure 33).



Figure 33. Pairs of coaxial rotors. Left: larger on top, smaller in the bottom. Right: smaller on top, larger in the bottom.

Air velocity from the upper rotor partially compensates pressure difference near the lower rotor. The scheme of rotor location (Figure 34) is most inefficient when a smaller rotor is located on top. Upper rotor is smaller than the lower one and air flow from the smaller does not allow the larger rotor (that creates two times higher lifting force when it is standing separately) create a possible thrust. Thus, when the larger rotor is located on top and the smaller one in the bottom, higher lifting force is created than in case of rotor location vice versa. Also, when rotors have different weights, they create a different rotating moment that should be compensated with different rotation speeds of rotors in pair. This makes control of UAV more complex.

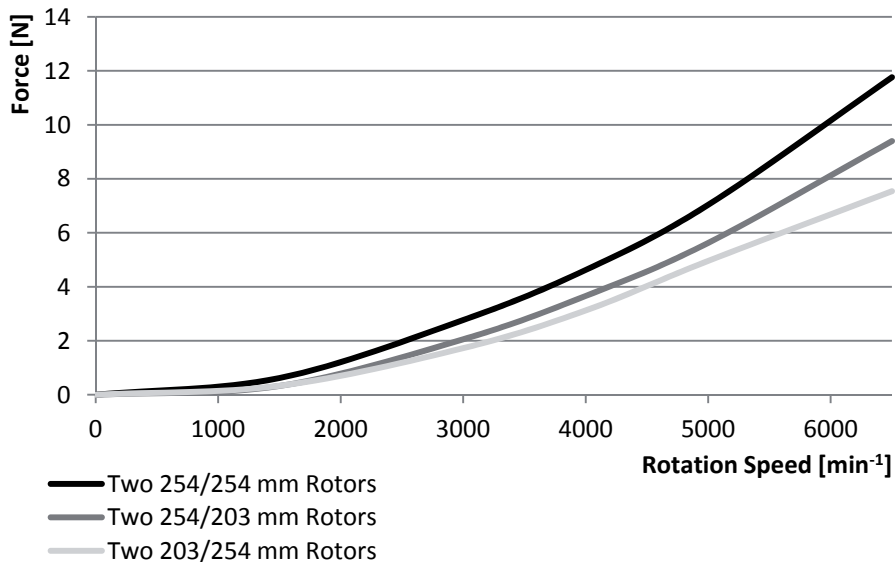


Figure 34. Dependency of the produced lifting force on the rotor rotation speed for three variants of coaxial rotor location.

CFD simulation results show that two coaxial rotors with same size produce about 21 % less lifting force than those staying separately. Because the flow from the upper rotor partially compensates the pressure near the lower rotor, it creates two times less force than the upper rotor. With the upper rotor larger than the lower one, the efficiency of the rotor pair is higher and vice versa.



### 3.2 Shrouded rotors

#### Shrouded rotors

Sometimes quadrotor helicopters are enclosed within a protective frame (Figure 35) permitting flights indoors and in obstacle-dense environments with reduced risk of damage to the vehicles, their operators, or surroundings. Those rotors with a rim around are usually called shrouded rotors or ducted fans. These added safety benefits greatly accelerate the design and test flight process by allowing testing to take place indoors or out, by inexperienced pilots, and with a short turnaround time for recovery from incidents [42]. Those shrouds around rotors can be also used to change properties of air flow around and near the rotor. Pressure difference between upper and lower surfaces can be changed and therefore adjusted lifting force is produced by the rotor and it will verify how changing parameters of closed rings around rotors affect the lifting force [51].



Figure 35. Quadrotor helicopter with a safety frame. AR Drone by Parrot.

#### Theory of shrouded rotor

According to Rankine–Froude momentum theory (rotor is modeled as an infinitely thin disc, inducing a constant velocity along the axis of rotation), the thrust of a propeller ( $T$ ) at hovering flight is given by Eq. (16) [62].

$$T = \frac{1}{2} \rho S_l V_e^2, \quad (16)$$

where

$\rho$  – air density,

$S_l$  – the disk rotor area (Figure 36-a),

$V_e$  – velocity of the air stream coming out.

With a shrouded fan, direct application of the momentum theory ensures the following:

$$T = \rho S_e V_e^2 = \sigma \rho S_1 V_e^2, \quad (17)$$

where

$S_e$  – terminal section of the air flow (Figure 36-b),

$\sigma = S_e / S_1$  – diffusion factor.

As it is shown in Eq. (16),  $\sigma$  is equal to 0.5 for a free propeller, and for a ducted-fan 20,  $\sigma$  is approximately equal to 1. For special ducts with spherical diffusors,  $\sigma$  can be greater than 3 or 5 [62].

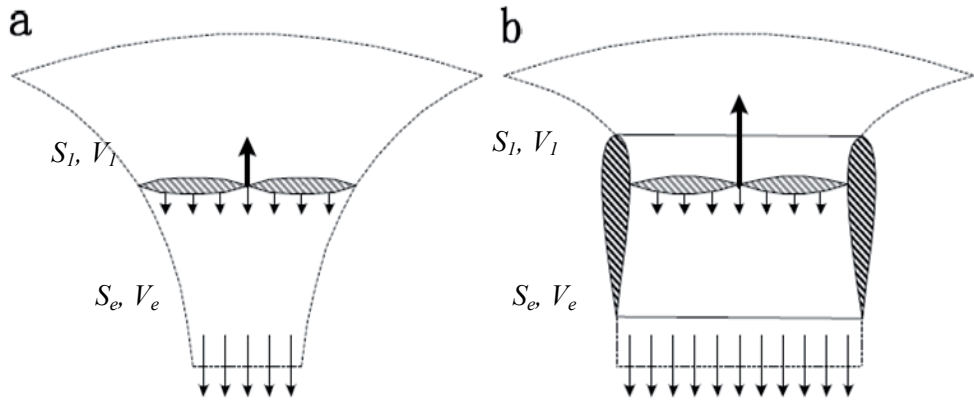


Figure 36. Air flow near the rotor without a duct (a) and with it (b) [62].

According to CFD optimization results [62], lifting force can be enlarged by using a duct that has conical geometry ( $S_e > S_1$ ).

This research has supplied a shroud with a shape of cylindrical tube around the rotor for safety purposes (for example, Safeflight Copters, USA). Minimal clearance between the rotor and the shroud is set to 3 mm. The use of a smaller clearance (less than 1 mm) rotor with a rim will work similarly to the impeller model [63]. In the impeller model the closeness of the internal rotor and the inner surface of the impeller housing minimizes turbulences created near the rotating rotor ends. Therefore, the lifting force will improve. In usual multi-rotor helicopters sufficiently flexible light materials (usually carbon fiber, plastic or styrofoam) are used. Creating stiff shroud around the rotor with a clearance less than 1 mm is not reliable (mass and/or price of helicopter will increase).

## Simulations

Simulations and experiments were conducted to understand how the closing rim affects the lifting force. It is possible to modify shroud dimensions to understand how its size affects the lifting force. Diameter was varying from 260 to 310 mm (Figure 37) while the rotor diameter used for simulations was 254 mm (10 in). The height of the shroud changed between 20 and 60 mm.

Firstly, simulations were made with CFD software to determine the lifting force. Lifting force produced by the rotor was determined at the rotor rotation speed of  $5000 \text{ min}^{-1}$  with a different diameter and height of the shroud. Next, in experiments the diameter of the shroud around the rotor was changed. Lifting force and motor power consumption were measured at different rotor angular velocities. Simulations and experiments for a case without a shroud around the rotor were done earlier.

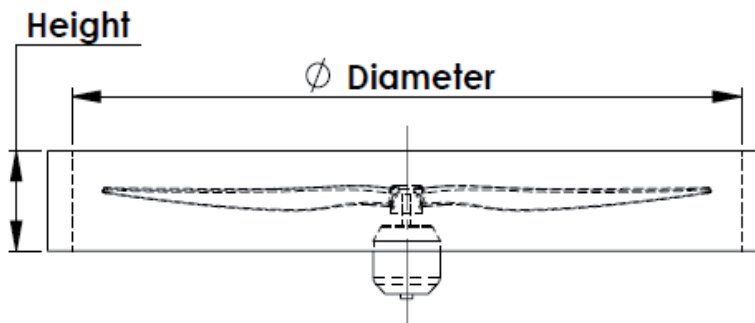


Figure 37. Changes of dimensions of the shroud around the rotor.

The lifting force created by rotors is calculated with the use of SolidWorks Flow Simulation. CFD results were also confirmed by experiments. In the simulation  $254 \times 127 \text{ mm}$  (diameter 10 in and pitch 5 inches) rotor was used as in previous simulations. In the series of simulations the rim diameter and its height were changed. All the simulations were made with a rotor angular velocity of  $5000 \text{ min}^{-1}$ .

Figure 38 shows the dependency of the lifting force produced by one rotor on a certain diameter of the shroud around it. Shroud's height is fixed to 40 mm. Minimum diameter is 260 mm (when the clearance between the rotor and the shroud is only 3 mm at each side) and maximum is 310 mm. The graph shows that with an increase in the shroud diameter the lifting force also increases. Dashed line shows the lifting force of the rotor without any shroud around it.

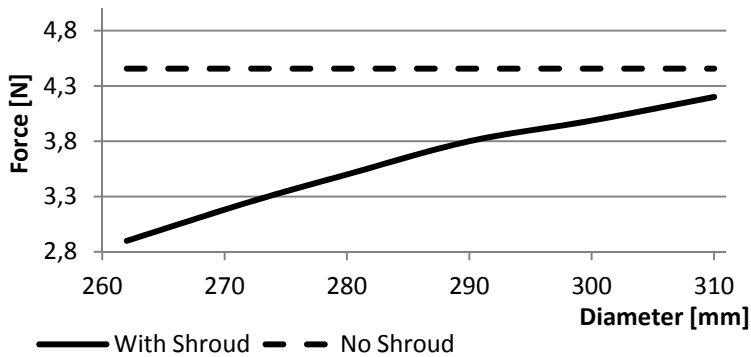


Figure 38. Dependency of the lifting force on the diameter of the shroud around the rotor.

Near the ends of the rotating rotor vortex areas are created. Those areas lead to the “overflow” of air from the higher pressure region near the bottom surface of the rotor to the lower pressure area near the top rotor surface. In Figure 39 the shroud diameter is 260 mm. When the shroud is maximally close to the rotor, turbulence on the rotor ends changes and the vortex goes around the shroud. In Figure 33 colors show pressure, vectors show velocity direction and magnitude of the flow.

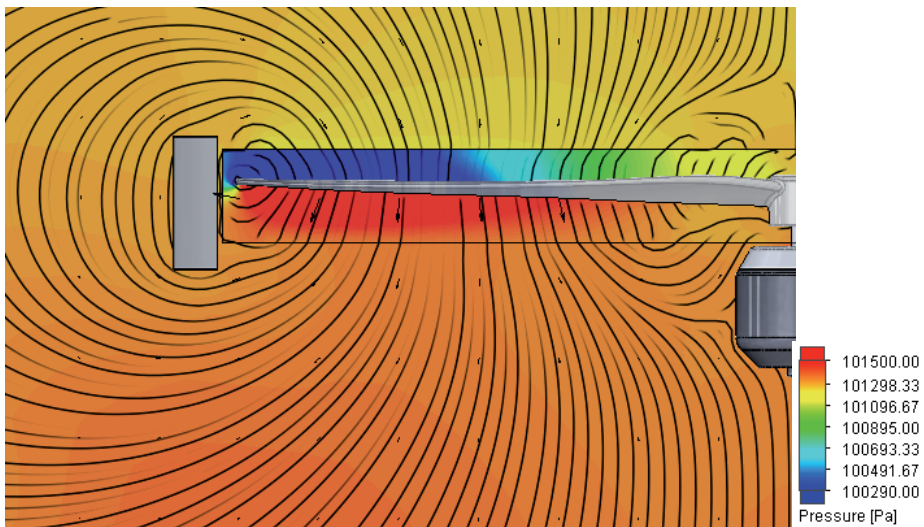


Figure 39. Pressure (colors) and velocity (vectors) distribution around the rotating rotor with the shroud with a diameter of 260 mm.

The rotor is surrounded by the shroud with a larger diameter (Figure 40) vortex flow near the rotor ends goes around the rim only partly. With an increase of the shroud diameter, the rotor works more like a separately standing (with no shroud) rotor.

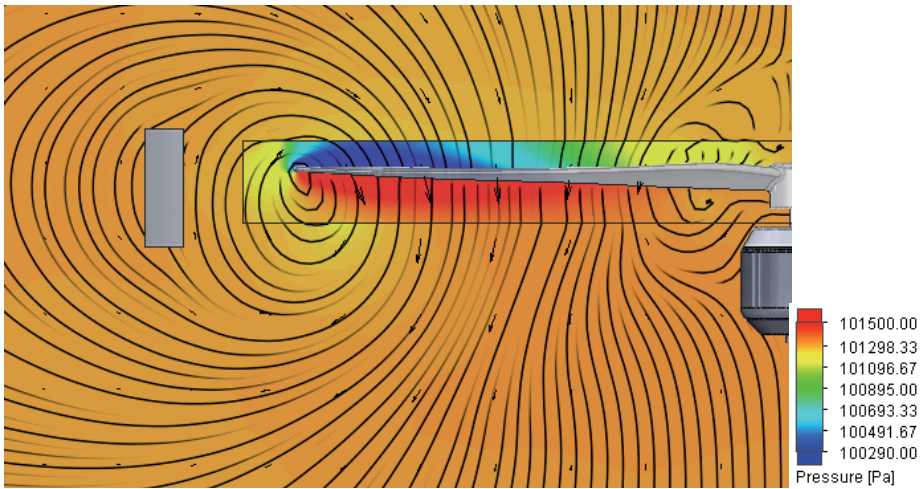


Figure 40. Pressure (colors) and velocity (vectors) distribution around the rotating rotor with a shroud diameter of 310 mm.

By changing the height of the shroud (Figure 41), the lifting force is decreasing from the height of 20 mm to 28 mm and then increases to 40 mm. At the start of this point the lifting force stays on same level with a future increase of the shroud height. At a larger height, the vortex there moves to the inside of the formed tube (Figure 42) and this promotes a decrease of pressure difference reduction between the upper and lower surfaces of the rotor.

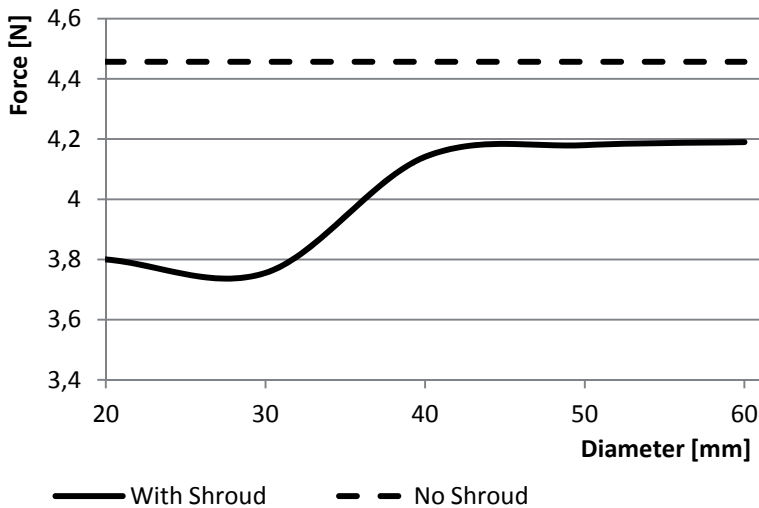


Figure 41. Dependency of the lifting force on the height of the shroud around the rotor.

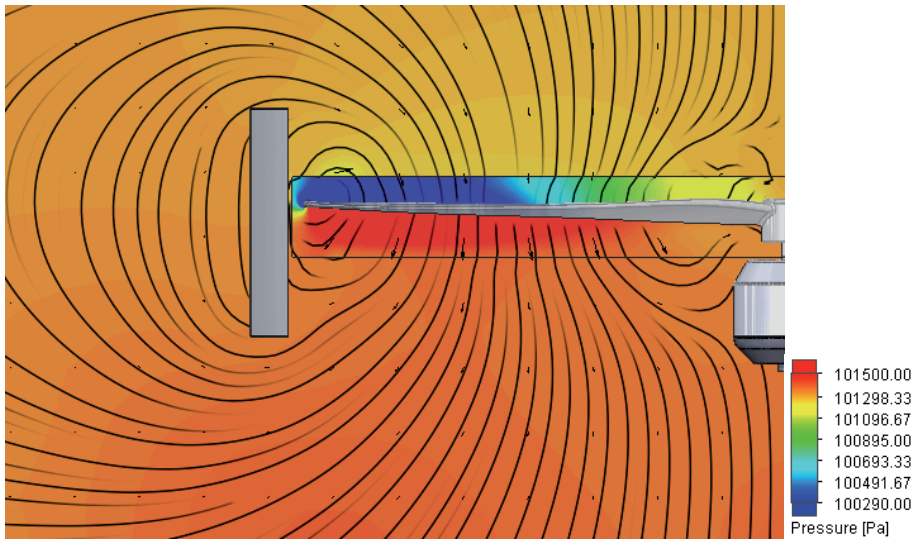


Figure 42. Pressure (colors) and velocity (vectors) distribution around the rotating rotor with a shroud height of 60 mm.

## Experiments

In experiments the same motor, rotor, controller and other components used before in experiments were employed. A shroud with a height of 60 mm and changeable diameter was made from steel sheet metal and fixed by three support stands (Figure 43). Altogether measurements for five different diameters of the shroud were made. Simulations and experiments without a shroud around the rotor were done earlier.

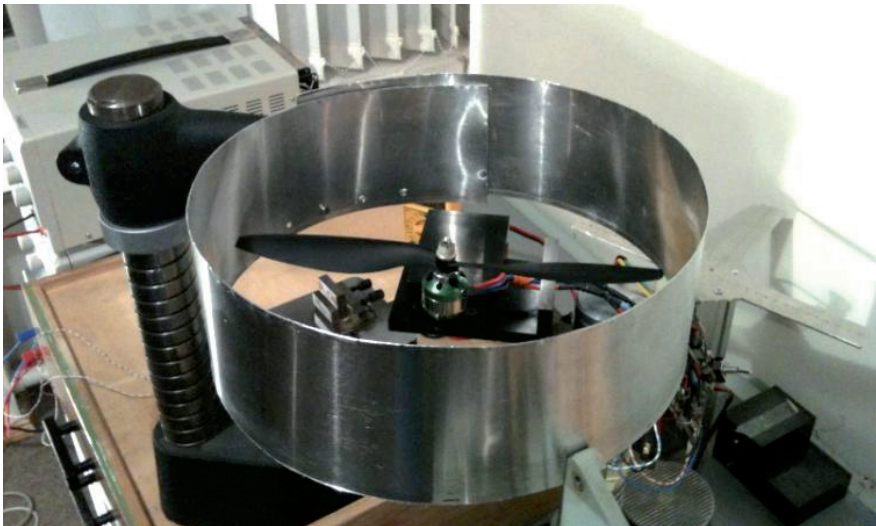


Figure 43. Experiments.

The graph in Figure 44 shows the dependency of the lifting force on rotor angular velocity for different diameters of the shroud around the rotor (average  $R^2 = 0.986$ ). With the magnification of the shroud diameter, the lifting force produced by the rotor also increases. Designs with no shroud around the rotor are most effective. Graphs in Figures 45 and 38 are similar, with data obtained from experiments (at the rotor angular velocity of  $5000 \text{ min}^{-1}$ ,  $R^2 = 0.99$ ). Dependencies obtained by simulations and experiments are very close.

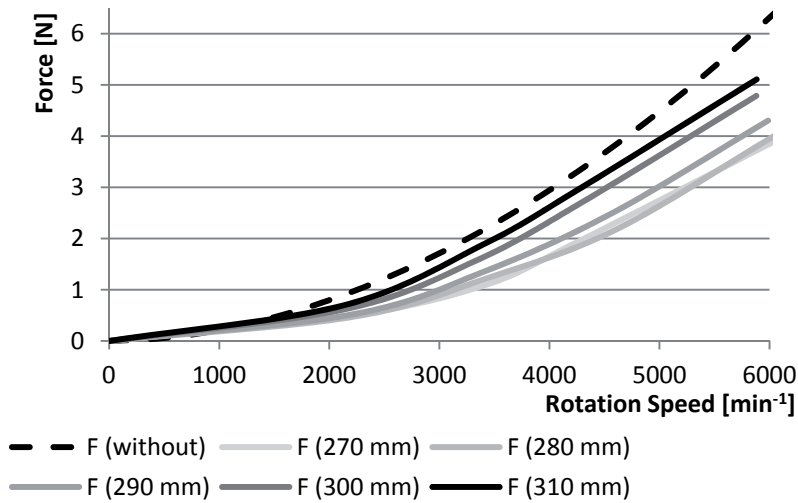


Figure 44. Experiments. Dependency of the lifting force on the rotor rotation speed for different diameters of the shroud around the rotor.

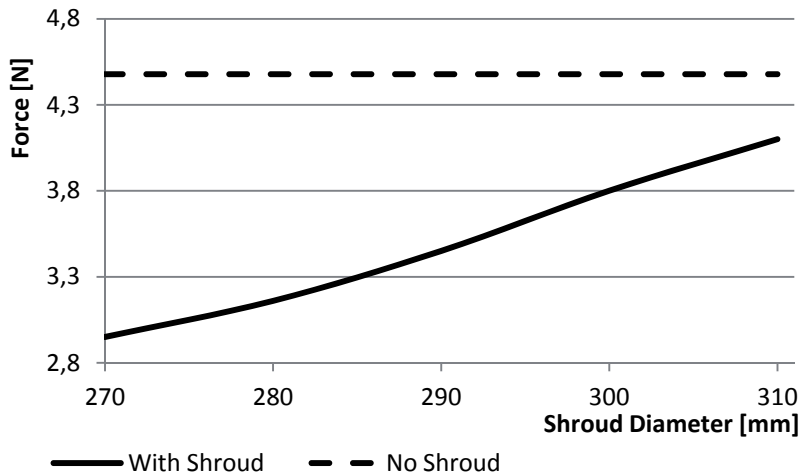


Figure 45. Experiments. Dependency of the lifting force on the diameters of the shroud around the rotor.

During experiments, power consumption measurement was also made using a bypass resistor. Figure 46 shows the dependency of the lifting force on the motor's power consumption (average  $R^2 = 0.978$ ). With the magnification of the rim, the diameter force to the efficiency of power consumption also increases. Rotating rotor creates the highest lifting force when the shroud around the rotor is not used as compared to other designs at the same motor power consumption.

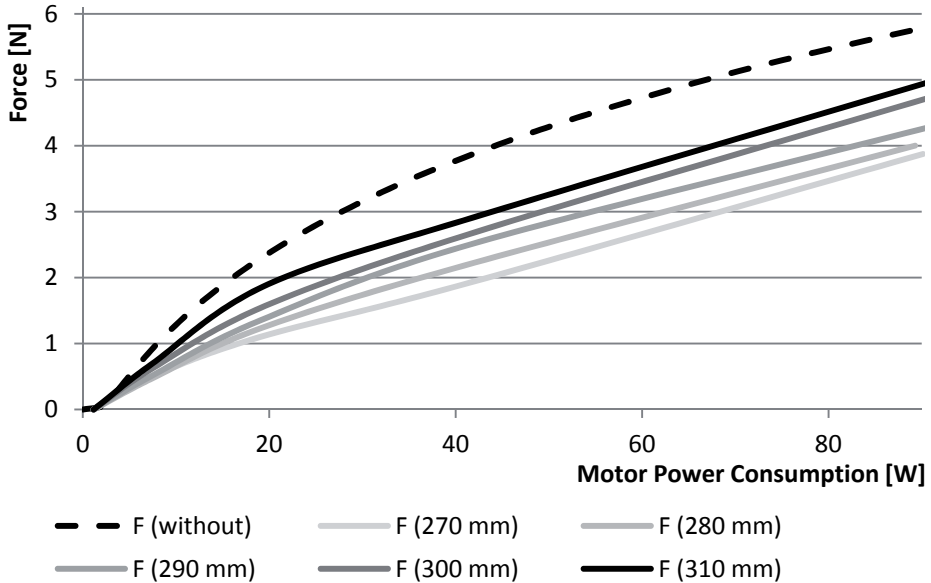


Figure 46. Experiments. Dependency of the lifting force on the motor power consumption.

Changing diameter of the shroud leads to the lifting force also changing. The smaller the shroud diameter, the smaller lifting force can be produced at certain angular velocity and certain motor power. With an increase in the shroud height the lifting force increases up to 40 mm height and then stabilizes (similar to the rotor working in a long tube). The lifting force of a rotor with different diameter and height dimensions of straight safety shroud around it is less than the force produced by the rotor without the shroud.



### 3.3 Comparison of multicopters with a different number of rotors

#### Theory of multicopter movement

Next, the mathematical models of multicopters with a different number of rotors are compared. Time of immovable hovering of UAVs and their linear motion flight duration time were compared. In the analysis, the same copter principle and characteristics (size, motors, rotors, battery and others) were used.

To understand how UAVs with different numbers of rotors move in space, we assume that there are two reference frames, the earth frame (E-frame) represented by the variables  $x, y, z$ , and the multicopter frame (M-frame) represented by the variables  $X, Y, Z$ . Both of these frames follow the right-handed coordinate system. The origin of the M-frame is attached to the center of the mass of the aircraft. The positive  $X$ -axis points towards the front of the airframe, the positive  $Y$ -axis points towards the left and the positive  $Z$ -axis is directed in an upward direction (Figure 47). The positive sense of the three Euler angular variables, roll ( $\varphi$ ), pitch ( $\theta$ ) and yaw ( $\psi$ ) is decided by the right-handed rotation about the positive  $x, y$ , and  $z$  axes, respectively [82, 83].

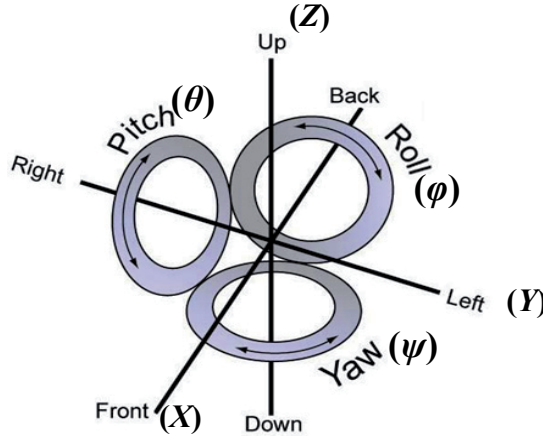


Figure 47. M-frame coordinate system, picture from <http://weboflife.nasa.gov>.

Aircraft is represented with 6 degrees of freedom with respect to the earth inertial frame E. The coordinates of the aircraft are as follows [82]:

$$q = (P, A) \in R^6, \quad (18)$$

where

$P = (x, y, z) \in R^3$  is the vector which denotes the position of the center of the mass of a helicopter with respect to the frame E,

$A = (\theta, \psi, \varphi) \in R^3$  – three angles of the rigid body in the fixed frame M.

The dynamic model of a multicopter is obtained via the Euler–Lagrange equations as follows [82]:

$$\frac{d}{dt} \frac{\partial L}{\partial \dot{q}} - \frac{\partial L}{\partial q} = F, \quad (19)$$

where

$L$  – Lagrangian function,

$F = (F_p, \tau)$ ,

$F_p = (F_x, F_y, F_z)^T$  – external lift force applied to aircraft,

$\tau = (\tau_x, \tau_y, \tau_z)^T$  – external torque.

To change the orientation of a helicopter by the rotation of a rotor, we need to transform it with respect to the earth inertial frame E, Eq. (20) [82].

$$F_p = R \cdot \begin{bmatrix} 0 \\ 0 \\ \sum_{i=1}^n F_i \end{bmatrix}, \quad (20)$$

where

$F_i$  – lift force generated by each motor ( $i = 1, 2, 3..$ ),

$n$  – number of rotors,

$R$  – transformation matrix from the earth inertial frame E, Eq. (21).

$$R = R_z \cdot R_y \cdot R_x = \begin{bmatrix} c\theta \cdot c\psi & s\varphi \cdot s\theta \cdot c\psi - c\varphi \cdot s\psi & c\varphi \cdot s\theta \cdot c\psi + s\varphi \cdot s\psi \\ c\theta \cdot s\psi & s\varphi \cdot s\theta \cdot s\psi + c\varphi \cdot c\psi & c\varphi \cdot s\theta \cdot s\psi - s\varphi \cdot c\psi \\ -s\theta & c\theta \cdot s\varphi & c\theta \cdot c\varphi \end{bmatrix}, \quad (21)$$

where

$c$  – cosinus abbreviation,

$s$  – sinus abbreviation.

A equation of the total lift force is presented in Eq. (22) [82, 83].

$$F_p = \begin{bmatrix} c\varphi \cdot c\psi \cdot s\theta + s\varphi \cdot s\psi \\ c\varphi \cdot s\psi \cdot s\theta - s\varphi \cdot c\psi \\ c\varphi \cdot c\theta \end{bmatrix} \sum_{i=1}^n F_i. \quad (22)$$

### Comparison of multicopters

To unify our models we will compare helicopters with the same motors and rotors. Mass of the platform is combined from 1080 g – platform base (including body, battery, controller and other equipment) and each rotor system mass – 80 g (including 57 g motor, rotor, ESC, wiring and other component masses). Centers of helicopter masses are located in the centers of the models. Also, idealized room conditions without winds are used. It is taken into account that torques ( $\tau$ ) from different rotors compensate each other.

To hold aircraft immovable in the air, all rotors must rotate at the same speed and create a force that compensates the weight of the platform. For a horizontal flight helicopter, it must slope in the direction of flight. All motors and rotors are immovable in relation to the body of a UAV and when the platform is sloped, forces from rotors also slope (pitch) around the  $Y_m$  axis ( $F_p$ ,  $\theta$  in Figure 48).

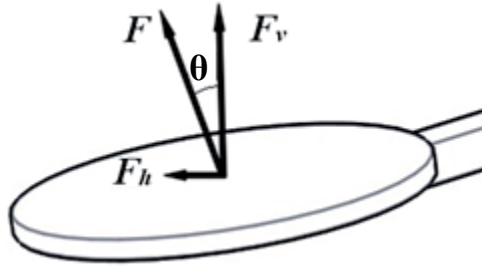


Figure 48. Force distribution in the horizontal flight.

Decomposing the force  $F_p$  we obtain the vertical (lifting) force  $F_v$  and the horizontal (pulling) force  $F_h$ , Eq. (23).

$$F_v = F \cdot \cos\theta, \quad (23)$$

$$F_h = F \cdot \sin\theta,$$

where

$F$  – force produced by the rotor,

$\theta$  – slope angle.

To provide horizontal flight, the sum of all vertical forces must be equal to the gravity force. The horizontal forces  $F_h$ , in the absence of air resistance, accelerate the helicopter. Eq. (24) gives the horizontal force that is needed to accelerate the helicopter from 0 to the velocity  $v$  within the distance  $\Delta S$ . Here we take into account that our platform is moving forward at a velocity of 2 m/s on distance 1 m.

$$F_h \cdot \Delta S = \frac{m \cdot v^2}{2},$$

$$F_h = \frac{m \cdot v^2}{2 \cdot \Delta S}, \quad (24)$$

where

$\Delta S$  – movement, m,

$m$  – mass, kg,

$v$  – velocity, m/s,

$F (F_h)$  – force (pulling), N.

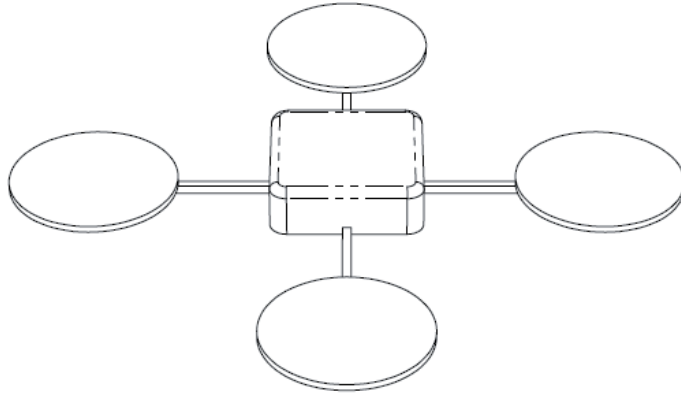


Figure 49. Four-rotor helicopter.

Overall mass of a four-rotor multicopter (Figure 49) is 1.4 kg and 3.5 N force must be created by each rotor to hold the aircraft in air in the horizontal direction and to reach this force 177.6 W (experiments measurement error is  $\pm 1.5$  W) of total power by four motors is needed.

For platform movement in the horizontal direction at a velocity of 2 m/s, a total of 2.8 N of  $F_h$  is needed (27). Each rotor needs to generate 0.7 N of this force. To reach those forces, an angle  $\theta$  of 11.3 degrees is needed, so the total force of each rotor is 3.57 N and to reach this force, 181.9 W of total multicopter power is needed. When the platform is sloped,  $F_v$  must be 3.5 N.

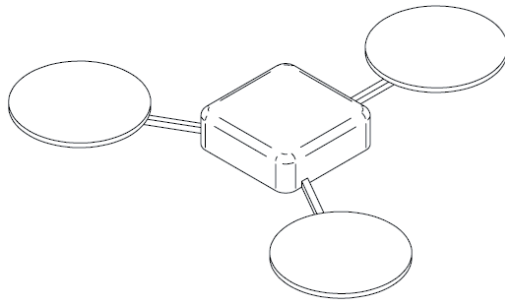


Figure 50. Three-rotor helicopter.

On a three-rotor helicopter – tricopter (Figure 50) with a mass of 1.32 kg, each rotor must reach 4.4 N (total multicopter power is 177.1 W) to hold the platform immovable. For the horizontal flight, a pulling force of 2.64 N ( $F_h$ ) is needed and to reach this, each rotor must generate 0.88 N of this force. Those parameters can be kept when the slope angle is 11.31 degrees and 4.49 N force is produced by each rotor.

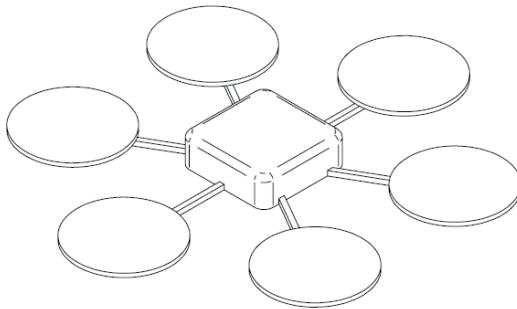


Figure 51. Six-rotor helicopter.

A six-rotor helicopter – hexacopter (Figure 51) must generate 2.6 N of force by each rotor (total power consumption 183.9 W). To reach the horizontal flight velocity of 2 m/s, each rotor must generate 2.65 N force.

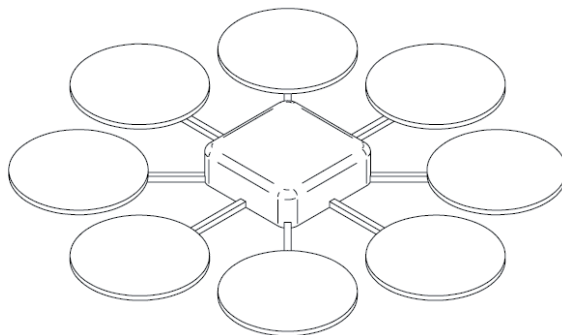


Figure 52. Eight-rotor helicopter.

An eight rotor helicopter – octocopter (Figure 52) uses eight separately standing rotors. To hold an aircraft with a mass of 1.72 kg in the air, each rotor must generate 2.15 N lifting force and 193.5 W of total power consumption is needed.

#### Comparison of multicopter power consumption

To calculate helicopter power consumption, experiment data described in section 2.1 were used. The calculation involved only power consumption of motors. Power consumption of the main controller, RC module (Radio Control) and other devices were not taken into account. In flight duration calculations a battery with a capacity of 54 Wh was used. Table 1 presents calculation data about all several rotor helicopters compared – rotor rotation speed, produced lifting forces, power consumption, flight duration time and other data. Motor power consumption experiment measurement error is  $\pm 1.5$  W and rotor speed error is  $\pm 34$   $\text{min}^{-1}$ . Flight duration calculation error is  $\pm 0.3$  min. Time and force that is needed to slope a UAV is not taken into account.

Table 1. Results of flight duration calculation for multicopters.

	N of rotors	3	4	6	8
	Helicopter mass, g	1320	1400	1560	1720
	Fv each rotor, N	4.4	3.5	2.6	2.15
	Fh each rotor, N	0.88	0.70	0.52	0.43
Hovering	Rotor speed, $\text{min}^{-1}$	4954	4387	3746	3386
	One rotor power, W	59.1	44.4	30.7	24.2
	Total power, W	177.1	177.6	183.9	193.5
	Time, min	18.3	18.2	17.6	16.8
Horizontal Flight	Rotor speed, $\text{min}^{-1}$	5005	4433	3785	3422
	One motor power, W	60.5	45.5	31.4	24.8
	Total power, W	181.5	182.0	188.4	198.3
	Time, min	17.9	17.8	17.2	16.3

Figure 53 presents a comparison of flight time for helicopters with different numbers of rotors. Both, hovering and horizontal flight durations are presented on one chart. Horizontal flight time is slightly shorter than hovering time. Mathematically, tricopter and quadcopter are the most efficient helicopter types, but for tricopter stabilization, an additional servo motor needed that would slope the tile rotor for compensating the rotating moment. Flight time of six- and eight-rotor helicopters compared to quadcopter is smaller

respectively 3 % and 8 % because the motor power consumption curve is non-linear and the mass of the device is greater. Most optimal type of a multicopter is a quadrocopter, that will be used for following calculations.

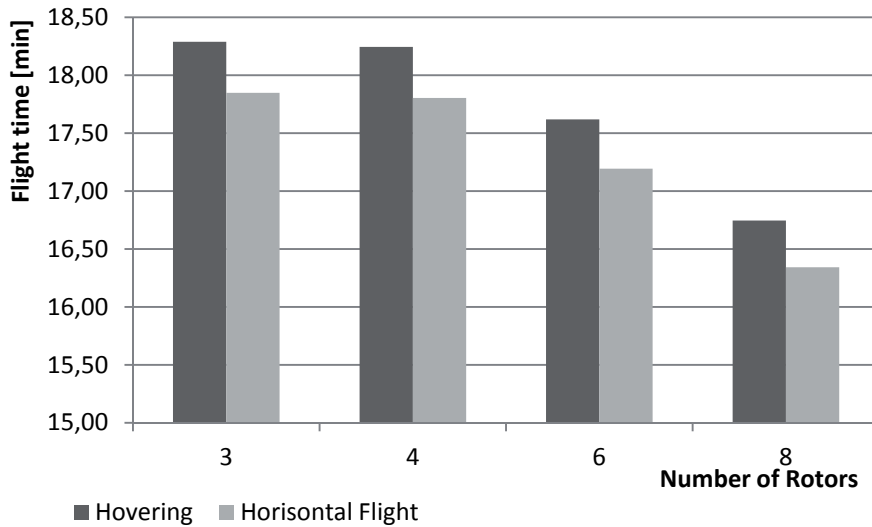


Figure 53. Comparison of hovering and horizontal flight time duration.

## 4. OPTIMAL DISTANCE BETWEEN ROTORS

### 4.1 Influence of distance between the rotors on the lifting force

The laminar and turbulent flows are created near the rotating rotor. In the flying platforms, rotors are located close to each other and flows are combining. When rotors are very close to each other, flows from them hardly affect neighboring rotors and their motor power consumption. At large distances between the rotors, the mass and dimensions of a helicopter increase because of lengthening of the central cross. It is required to determine an optimal distance between the rotors when the helicopter mass is at minimum and rotors are creating a maximum lifting force – air flows affect each other minimally.

To determine optimal distances, lifting forces of four rotor flying platforms (mini UAV) with different distances between rotors were analyzed. The air outflows from the rotors that affect each other in a quadrotor helicopter (quadcopter) were simulated and the lifting force was determined with CFD software. Helicopters with different distances between the rotors at different angular velocities were compared. Also, similar experiments were done. A testing device for measurement of real rotor angular velocity, lifting force and energy consumption of the motor was similar to that used in previous experiments.

#### Simulations

Simulations for lifting force determination and optimization of distance between rotors were conducted on a simplified quadrotor helicopter model with 254 mm (10 in) rotors. Separate simulations for different rotation speeds  $1500 \text{ min}^{-1}$ ,  $3000 \text{ min}^{-1}$ ,  $4000 \text{ min}^{-1}$  and  $5000 \text{ min}^{-1}$  were done. For each rotation speed distance range between the rotors changed from 5 mm to 140 mm (Figure 54).

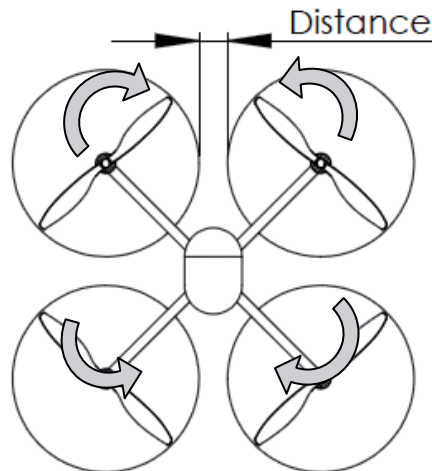


Figure 54. Simplified model of a quadrotor helicopter for CFD simulation. Directions of rotor rotation shown by arrows.



Results of the simulations show that the lifting force increases on distances from 5 mm to 35 mm (Figure 55) and this growth is around 15 %. From a distance of 70 mm the lifting force will decrease by around 2 % and then will stabilize. This level corresponds to a level of the lifting force produced by one separately working rotor.

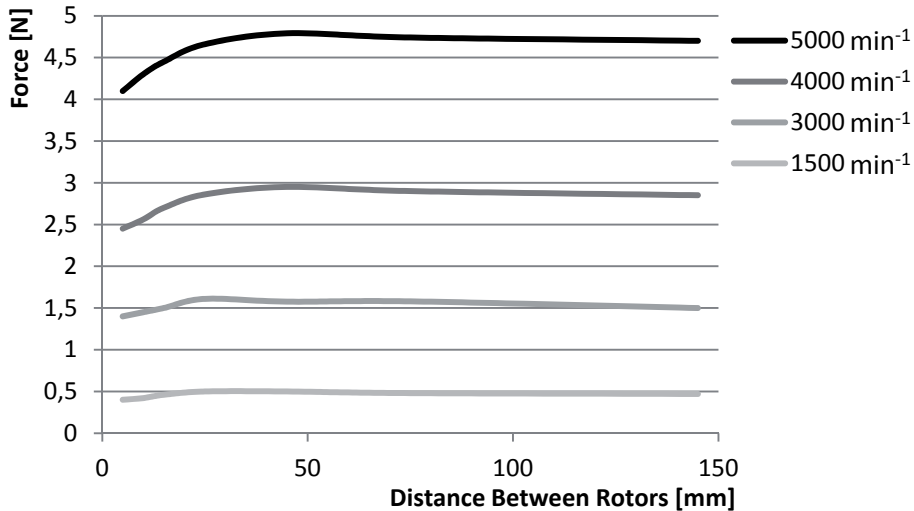


Figure 55. Dependency of the lifting force on the distance between the rotors for different rotation speeds of the rotor in the simulations.

Figure 56 shows air flow velocities and their directions of a quadrotor helicopter (front and top views) with 10 mm distance between the rotors. Velocity range is 0 – 13 m/s, darker areas near the rotor show higher velocities. Near the endings of the rotating rotor small turbulent areas appear where air flow is twisting upwards. In the space between the rotors there is a place where air flows are running into each other and the resulting flow moves upwards. This stream partially compensates the lifting force. Figure 57 illustrates air flow velocities and their directions of a quadrotor helicopter when the distance between the rotors is 140 mm. At this distance the influence of air flows from the rotors is insufficient and each rotor works as if it stayed separately.

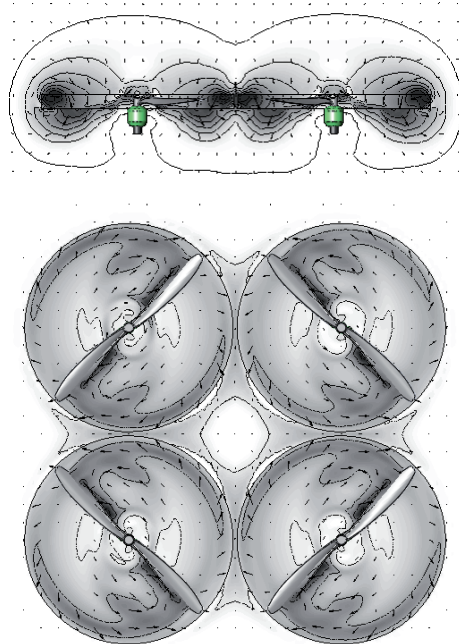


Figure 56. Air velocity distribution near the rotors, distance between the rotors 10 mm.

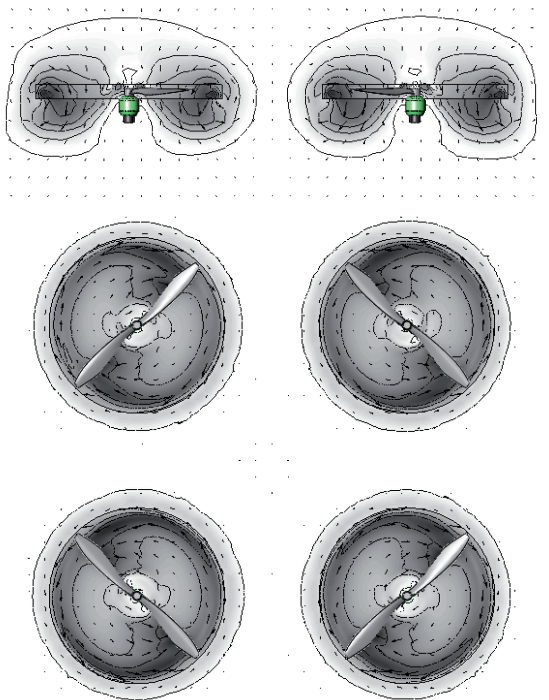
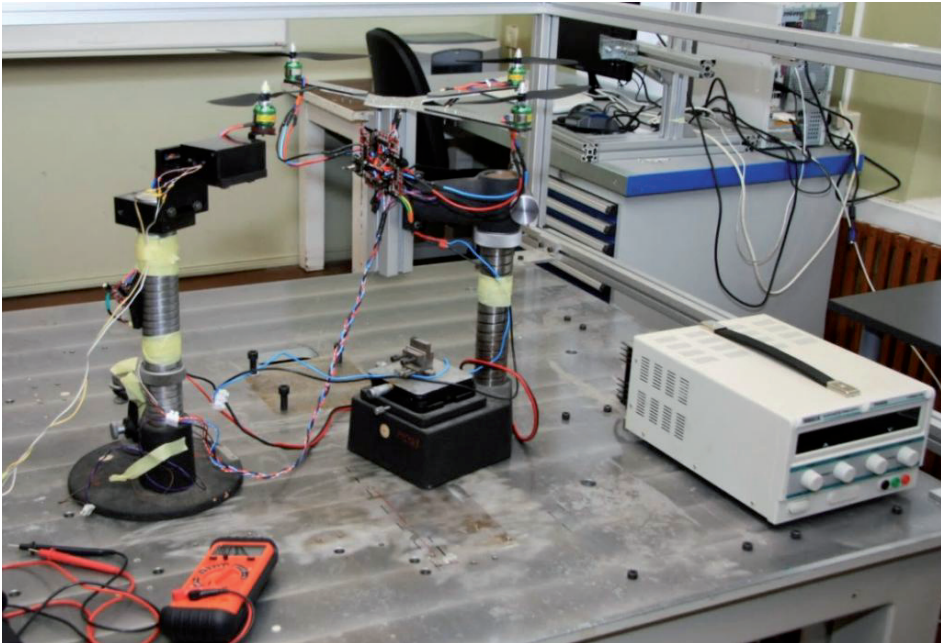


Figure 57. Air velocity distribution near the rotors, distance between the rotors 140 mm.

## Experiments

For experiments a testing device was designed that imitates a quadcopter with a capacity of changing the distance between the rotors (Figure 58). This device is based on a setup used for the determination of one rotor lifting force and it uses the same motors, rotors, motor control system and measurement devices. Additionally, nine custom details were made that allow distances to be changed between the rotors with a 10 mm increment. One of the four rotors was fixed on the force measurement device.



*Figure 58. Testing device imitates a quadcopter with an ability of changing distance between the rotors.*

Figure 59 illustrates the dependency of the lifting force on the distance between the rotors for different rotor angular velocities (average coefficient of determination for experiments  $R^2 = 0.985$ ). Data from the experiments and results of simulation are presented in one chart. Both of the methods gave approximately similar results (maximum difference is about 3 %). This confirms the validity of the results that can be used for the optimization of the distance between the rotors. At the same angular velocity of the rotor, it can produce different lifting forces on different distances between the rotors. Thus, a rotor rotating at rotation speed of  $5000 \text{ min}^{-1}$  produces 14.8 % higher lifting force on an optimal than at minimum distance.

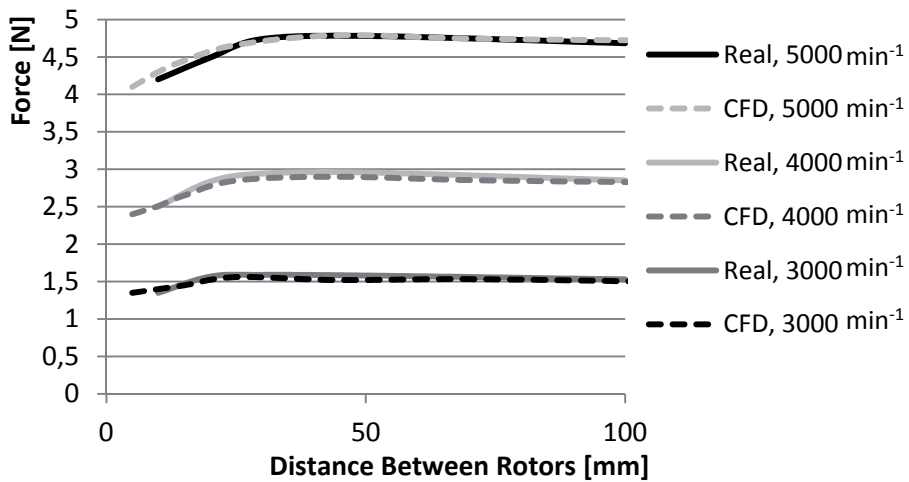


Figure 59. Dependency of the lifting force on the distance between the rotors for different rotation speeds. Comparison of experiments with the CFD simulations.

Motor power consumption is higher on a small distance between the rotors, then it falls (8 % – 10 %) and minimum is around 40 mm distance. Figure 60 shows the dependency of motor power consumption on the distance between the rotors for different lifting forces produced by the rotor (average  $R^2 = 0.979$ ). Difference between an optimal and the highest power consumption is 9.7 % (without taking into account increasing mass of a quadcopter) while the rotor creates a lifting force of 5 N.

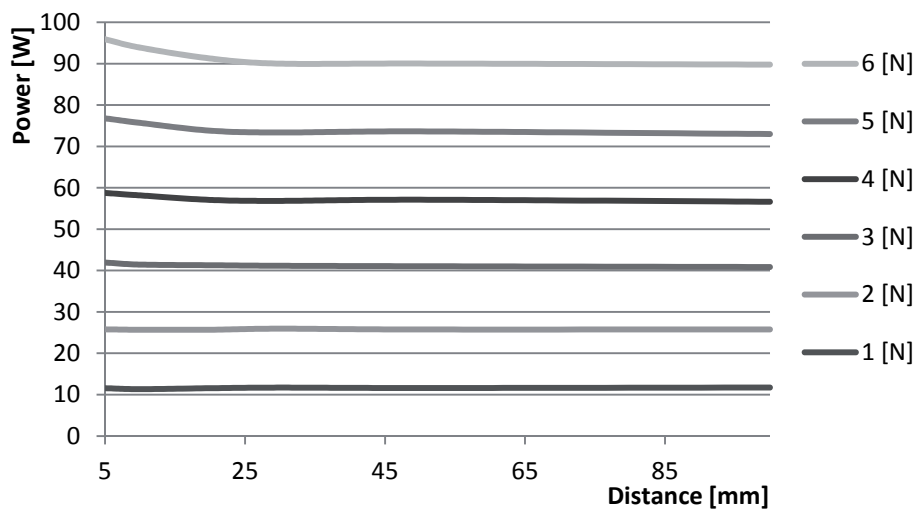


Figure 60. Dependency of motor power consumption on the distance between the rotors.

## 4.2 Optimal distance determination

Optimal distance between the rotors is the distance when the rotors are creating a maximum lifting force – air flows affect each other minimally. The optimal distance between the rotors of a quadrotor helicopter must be considered in hover. Mass of a newly created helicopter is usually known. This allows easy determination of the amount of the lifting force needed to be created by each rotor.

Data from CFD simulations are presented to show velocity dependency of the distance (see Figure 59). To determine an optimal distance needs to know the quantity of energy to produce a certain amount of lifting force. Since it is impossible to determine real energy consumption in future by the CFD software, we will use rotor's angular velocity that corresponds to the motor power consumption (section 2.2). To convert data, nonlinear regression analysis was made using Microsoft Excel Analysis ToolPack. Results are shown in Figure 61 where graphs show the level that an angular velocity motor needs to reach to create a certain amount of lifting force on a certain distance between the rotors. For example, to create a 5 N lifting force, a rotor needs to reach the rotation velocity of  $5698 \text{ min}^{-1}$  on a 5 mm distance and only  $5319 \text{ min}^{-1}$  on 41 mm.

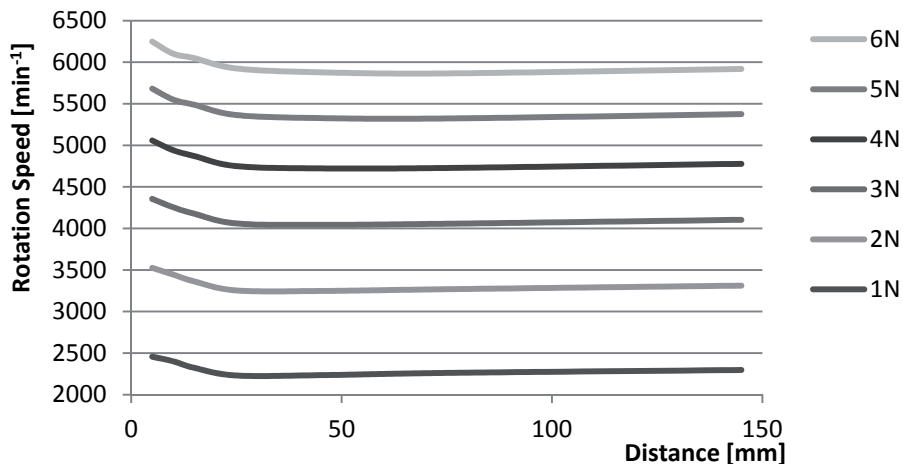


Figure 61. Dependency of the rotor rotation speed on the distance between the rotors. A rotor is producing a certain amount of lifting force.

For precise determination of the optimal distance the mass of the structure suspending the rotors has to be taken into account. It is assumed that the mass per length of the girder is  $0.25 \text{ g/mm}$ . Thus, when the distance between the rotors increases, the mass of the quadrotor helicopter also increases and more lifting force is needed to hold it immovable in air. Figure 62 shows the dependency of the rotor angular velocity on the distance between the rotors for creating a 5 N of lifting force. In this case, the optimal distance is 41 mm.

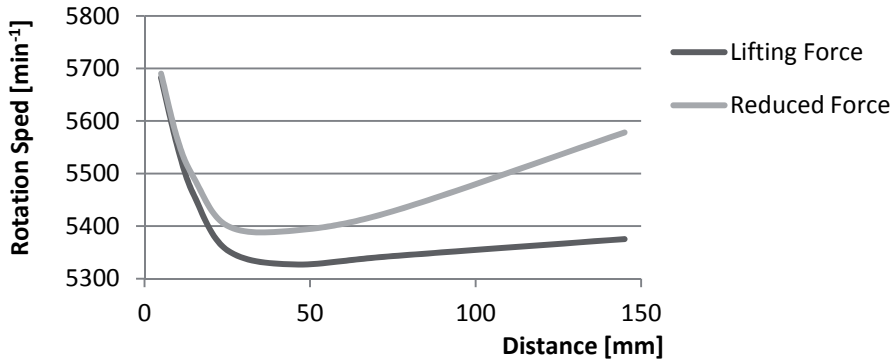


Figure 62. Optimal distance between 254 mm (10 in) rotors when they produce 5 N force.

254 mm (10 in) rotors have different optimal distances between the rotors at different rotation speed. They use the same data obtained from non-linear regression (Figure 61) to find optimal distances that correspond to different lifting forces (Figure 63). Distance on the dependency of the lifting force for 254 mm (10 in) rotors is described by Eq. (25), coefficient of determination  $R^2 = 0.99$ .

$$L = 0.55 \cdot F^2 - 0.24 \cdot F + 29.75, \quad (25)$$

where

$L$  – optimal distance between 254 mm (10 in) rotors, mm.

$F$  – required one rotor lifting force for holding helicopter in hover, N.

and the coefficients with units are 0.55 mm/N<sup>2</sup>, 0.24 mm/N and 29.75 mm.

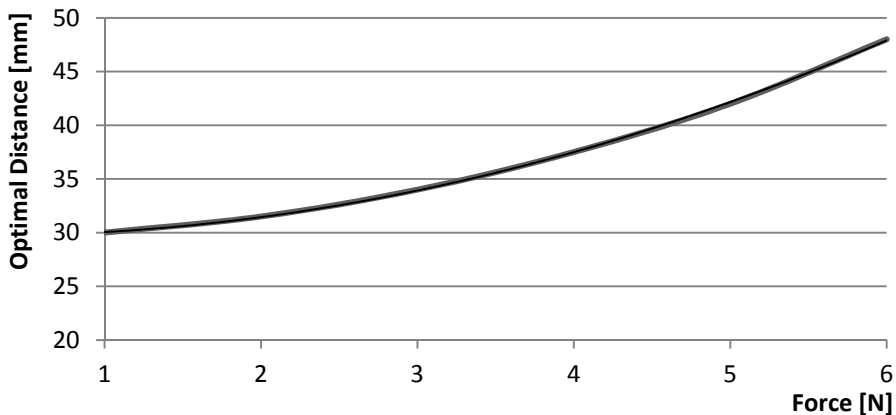


Figure 63. Optimal distances between 254 mm (10 in) rotors for different lifting forces.

To create the calculation method of mutual optimal distance, similar CFD simulations were done for the determination of the lifting force with different rotor diameters – 203.2 x 101.6 mm and 304.8 x 152.4 mm (8 x 4 in and 12 x 6 in respectively) rotors. Those simulations were done on different distances between the rotors and different angular velocities with the same parameters that were used for 254 mm (10 in) rotor simulations. Figure 64 shows the comparison between the lifting forces produced by three different rotors at the angular velocity  $5000 \text{ min}^{-1}$ .

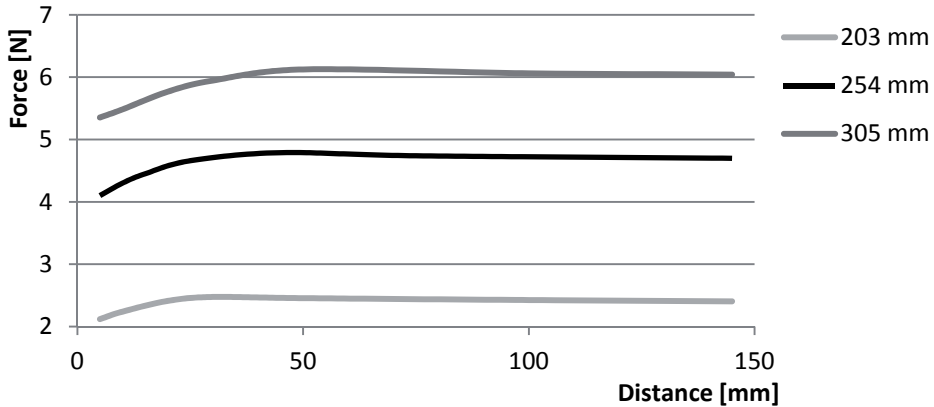


Figure 64. Lifting force produced by the rotor with the rotation speed  $5000 \text{ min}^{-1}$  on a certain distance between the rotors.

Optimal distances depending on the rotor diameter for different lifting forces are presented in Figure 65. This graph shows that dependencies of 2 N, 4 N, and 6 N lifting force are parallel. Overall dependency can be described by Eq. (26) (coefficient of determination  $R^2 = 0.99$ ).

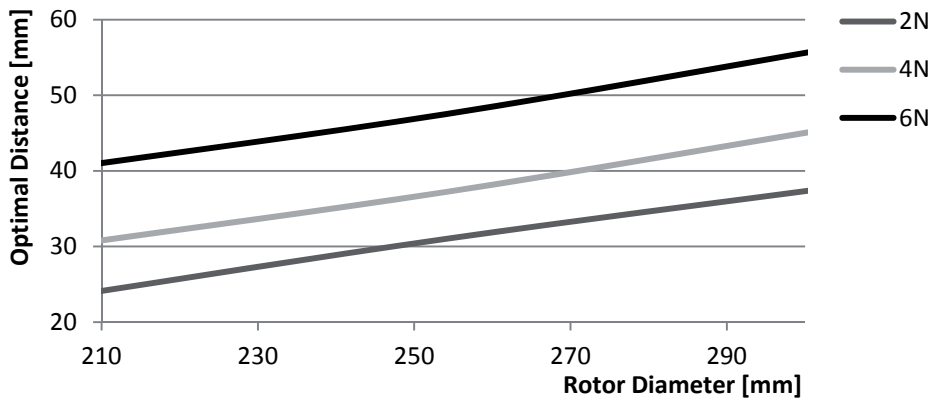


Figure 65. Optimal distances between rotors with different diameters (for creating force 2 N, 4 N and 6 N).

$$L_d = 0.15 \cdot D - 38.10, \quad (26)$$

where

$L_d$  – optimal distance dependency between the rotors, mm,

$D$  – rotor diameter, mm.

Combining Eqs. (25) and (26) we obtain Eq. (27), coefficient of determination  $R^2 = 0.97$ . Using this formula it is possible to find an optimal distance between the rotors in a quadrotor helicopter that uses rotors with a pitch equal to half of the diameter when one rotor's lifting force is known. The result of Eq. (27) is shown in Figure 66 on the 3-dimension graph.

$$L = 0.55 \cdot F^2 - 0.24 \cdot F + 0.15 \cdot D - 8.35, \quad (27)$$

where

$L$  – optimal distance between the rotors, mm,

$F$  – required one rotor's lifting force for holding helicopter in hover, N,

$D$  – rotor diameter, mm,

and the coefficients with units are  $0.55 \text{ mm/N}^2$ ,  $0.24 \text{ mm/N}$ ,  $0.15 \text{ mm}$  and  $8.35 \text{ mm}$ .

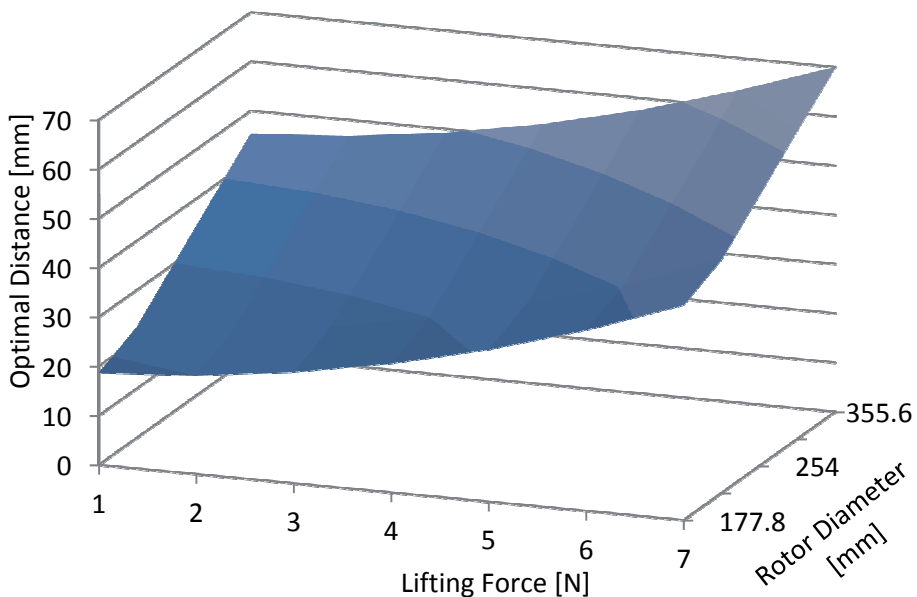


Figure 66. Optimal distances between the rotors.



To ensure that Eq. (27) is applicable to a large amount of rotors (not only when the rotor's pitch is equal to radius) pitch correction Eq. 11 ( $P_c$ ) is added and the result is Eqs. (28), coefficient of determination  $R^2 = 0.92$ .

$$\begin{cases} F_c = \left( P - \frac{D}{2} \right) \cdot (3.27 \cdot 10^{-4} \cdot D - 4.72 \cdot 10^{-2}) \\ L = 0.55 \cdot (F + F_c)^2 - 0.24 \cdot (F + F_c) + 0.15 \cdot D - 8.35 \end{cases}, \quad (28)$$

where

$F_c$  – pitch correction coefficient, N,

$L$  – optimal distance between the rotors, mm,

$F$  – required one rotor's lifting force for holding the helicopter in hover, N,

$D$  – rotor diameter, mm,

$P$  – rotor pitch, mm,

and the coefficients with units are  $3.27 \cdot 10^{-4}$  N/mm<sup>2</sup>,  $4.72 \cdot 10^{-2}$  N/mm, 0.55 mm/N<sup>2</sup>, 0.24 mm/N and 8.35 mm.

The coefficient of determination  $R^2 = 0.92$  gives a very precise result. Changing the optimal distance by  $\pm 8$  %, power consumption will change slightly, around 1 % because the rotor's rotation speed behavior is flat, near the optimal distance (Figure 56). Eq. (28) can be used within the rotor's diameter range 178 mm – 355 mm (7 in – 14 in) which the pitch is equal to 0.3 – 0.7 of the rotor diameter. Rotor's rotation speed must be within  $2000 \text{ min}^{-1}$  –  $8000 \text{ min}^{-1}$ .

To simplify the use of the resulting Eq. (31), widely used rotor sizes and masses of quadrotor helicopters are presented in Table 2. The table contains optimal distances (mm) between the rotor's rotation axes for different rotors, their pitches and masses of helicopters.

Theoretically this equation pair can be used not only for quadrotor helicopters, but also for multicopters with 3, 6, 8 and other number of rotors.

Table 2. Optimal distance (mm) between a rotor's rotation axes for different rotors and masses of quadcopters (*D* – diameter, *P* – pitch of rotor).

<b>D</b>	<b>P</b>	<b>D</b>	<b>P</b>	<b>Mass, g</b>								
mm	mm	in	in	1000	1250	1500	1750	2000	2250	2500	2750	3000
<b>178</b>	<b>89</b>	<b>7</b>	<b>3.5</b>	199	201	203	206	209	212	216	220	225
<b>178</b>	<b>102</b>	<b>7</b>	<b>4</b>	199	201	204	206	209	213	217	221	226
<b>178</b>	<b>114</b>	<b>7</b>	<b>4.5</b>	200	202	204	207	210	214	218	223	228
<b>203</b>	<b>102</b>	<b>8</b>	<b>4</b>	228	230	232	235	238	241	245	250	254
<b>203</b>	<b>191</b>	<b>8</b>	<b>7.5</b>	234	237	240	244	248	253	258	264	270
<b>229</b>	<b>114</b>	<b>9</b>	<b>4.5</b>	257	259	261	264	267	271	275	279	284
<b>229</b>	<b>152</b>	<b>9</b>	<b>6</b>	261	263	266	269	273	277	282	287	293
<b>254</b>	<b>94</b>	<b>10</b>	<b>3.7</b>	284	285	287	289	291	294	297	300	304
<b>254</b>	<b>119</b>	<b>10</b>	<b>4.7</b>	286	288	290	292	295	298	302	306	311
<b>254</b>	<b>127</b>	<b>10</b>	<b>5</b>	287	288	291	293	296	300	304	308	313
<b>254</b>	<b>152</b>	<b>10</b>	<b>6</b>	289	292	295	298	302	306	310	315	321
<b>279</b>	<b>140</b>	<b>11</b>	<b>5.5</b>	316	318	320	322	326	329	333	337	342
<b>279</b>	<b>165</b>	<b>11</b>	<b>6.5</b>	319	322	325	328	332	336	341	346	352
<b>305</b>	<b>114</b>	<b>12</b>	<b>4.5</b>	342	343	343	345	346	349	351	354	357
<b>305</b>	<b>152</b>	<b>12</b>	<b>6</b>	345	347	349	352	355	358	362	367	371
<b>305</b>	<b>178</b>	<b>12</b>	<b>7</b>	349	352	355	359	363	367	372	377	383
<b>356</b>	<b>152</b>	<b>14</b>	<b>6</b>	401	401	402	404	406	408	411	414	417
<b>356</b>	<b>178</b>	<b>14</b>	<b>7</b>	403	405	407	410	413	417	421	425	430
<b>356</b>	<b>203</b>	<b>14</b>	<b>8</b>	410	413	416	420	424	429	434	439	445

### 4.3 Methodology

This methodology provides recommendations for the design of the multicopter. Elements to be used in the multicopter are analyzed with regard to energy consumption. Also, step-by-step guidance for the determination of an optimal distance between the rotors according to the required lifting force, rotor diameter and pitch (Figure 67) is composed with the provision of sequence and types of activities.

Firstly, the use of separately standing rotors is more reliable. Due to the fact that in the coaxial rotor pair the flow from an upper rotor partly compensates the pressure difference near the lower rotor and leads to the reduction of the total lifting forces by 21 %. Shrouded rotors commonly used for safety reasons should not be used, if possible. The use of non-optimized shroud around the rotor with a relatively large clearance between the rotor tip and the shroud will increase the energy consumption of the motor.

Methodology for the determination of an optimal distance

1. Optimal distance between the rotors (one rotor size).

1.1 The number of rotors in the possible multicopter should be selected. Based on the research done, a quadcopter, a helicopter with four rotors, will be recommended. Since flows from rotating rotors affect each other at a sufficiently small distance, an optimal distance between rotor tips in multicopters with 4, 6, 8 and other number of rotors will be matching.

1.2 Scanning of three similar models of propellers with pitch equal to half of the diameter (2 other rotors will be needed for future steps).

1.3 First, simulation of the rotor lifting force on a simplified model of the multicopter using CFD software. Three different rotor rotation speeds from the range of usable speeds are sufficient. For the rotation speed of each rotor five measurements of the lifting force on different distances between the rotors are required. Simulation of three neighboring rotors is sufficient for an accurate result when using the typical simulation study. One rotor in the model is enough if software allows circular symmetry relation to be used.

Note: the 15 simulations recommended are very easy to reproduce using such SolidWorks functionality, like Configurations, Batch Run and Batch Result Processing.

Simulation in SolidWorks Flow Simulation can be done only in one direction, where the user defines rotor rotation speed and as a result obtains its lifting force. If the CFD software allows the rotation speed to be defined needed for a rotor to produce a certain amount of lifting force, continue with step number 1.5.

1.4 Definition of the dependence of the lifting force on the distance between the rotors for different propeller rotation speed from previous results (result similar to that in Figure 59).

1.5 Dependence of the rotor rotation speed on the distance between the rotors. The result enables the definition using nonlinear regression (for example Microsoft Excel) or directly from CFD software (see step 1.3). Five curves are needed (result similar to that in Figure 61).

1.6 Lower values from five graphs (obtained in 1.5) that correspond to a certain amount of lifting force are combined into a dependency. The dependency can be described as a quadratic equation and the results show the dependence of the distance between the rotors on the lifting force, result similar to that in Figure 63, Eq. (25).

2. Dependence of an optimal distance (for different rotor diameters).

2.1 If propellers of the same type are used (only diameters are different), the quadratic equation will be preserved with high level of confidence also for other diameters of rotors.

Next, the rotor of the second diameter (with the pitch of half the diameter) is used. From step 1.3 to 1.5, during the analyses it is necessary to obtain for this rotor an optimal distance for the one lifting force of it.

2.2 Using two points (from steps 1.5 and 2.1) the linear dependency of the optimal distance between the rotors on their diameter for a certain amount of the lifting force is defined.

2.3 Combining the quadratic equation from step 1.6 and linear from 2.2, the governing equation with two variables will be defined. This equation will represent the dependency of the optimal distance between the rotors on the required lifting force and propeller diameter, result similar to that in Figure 66, Eq. (27). The result will be valid when the rotor pitch equals half of the diameter.

3. Influence of the rotor pitch on the lifting force.

3.1 Determination of the influence of the rotor pitch on the lifting force. Using 3D modeling tools, it is necessary to create additional models of three scanned rotors with different pitches (larger and smaller than half the diameter), a total of three pitch sizes for each rotor.

3.2 Determination of a propeller's lifting force at a certain rotation speed with CFD software. Average velocity is taken from the expected range of usable velocities.

3.3 Finding of the linear dependency of the lifting force on the propeller pitch for each rotor diameter (in the form of  $ax + b$ , result similar to that in Figure 27, Eq. (9)).

3.4 Finding of linear dependency of  $a$  coefficient from step 3.3 from the rotor diameter. In the case of obvious non-linear dependency, steps 3.1 – 3.3 must be taken, additional two simulations for other diameters of the rotor and build a non-linear dependency. This will be the coefficient of the rotor's lifting force correction relative to the pitch equal to half the diameter, result similar to Eq. (11).

By multiplying the resulting equation by  $P - D / 2$  (where  $P$  is the rotor pitch and  $D$  is the rotor diameter), correction coefficient will have negative, zero or positive value, whereas the pitch is less, equal or larger than half the diameter.

As a result, using the combination of equations from 2.3 and 3.4 it is possible to obtain the optimal distance between the rotors in the multicopter knowing the required lifting force, rotor diameter and pitch.

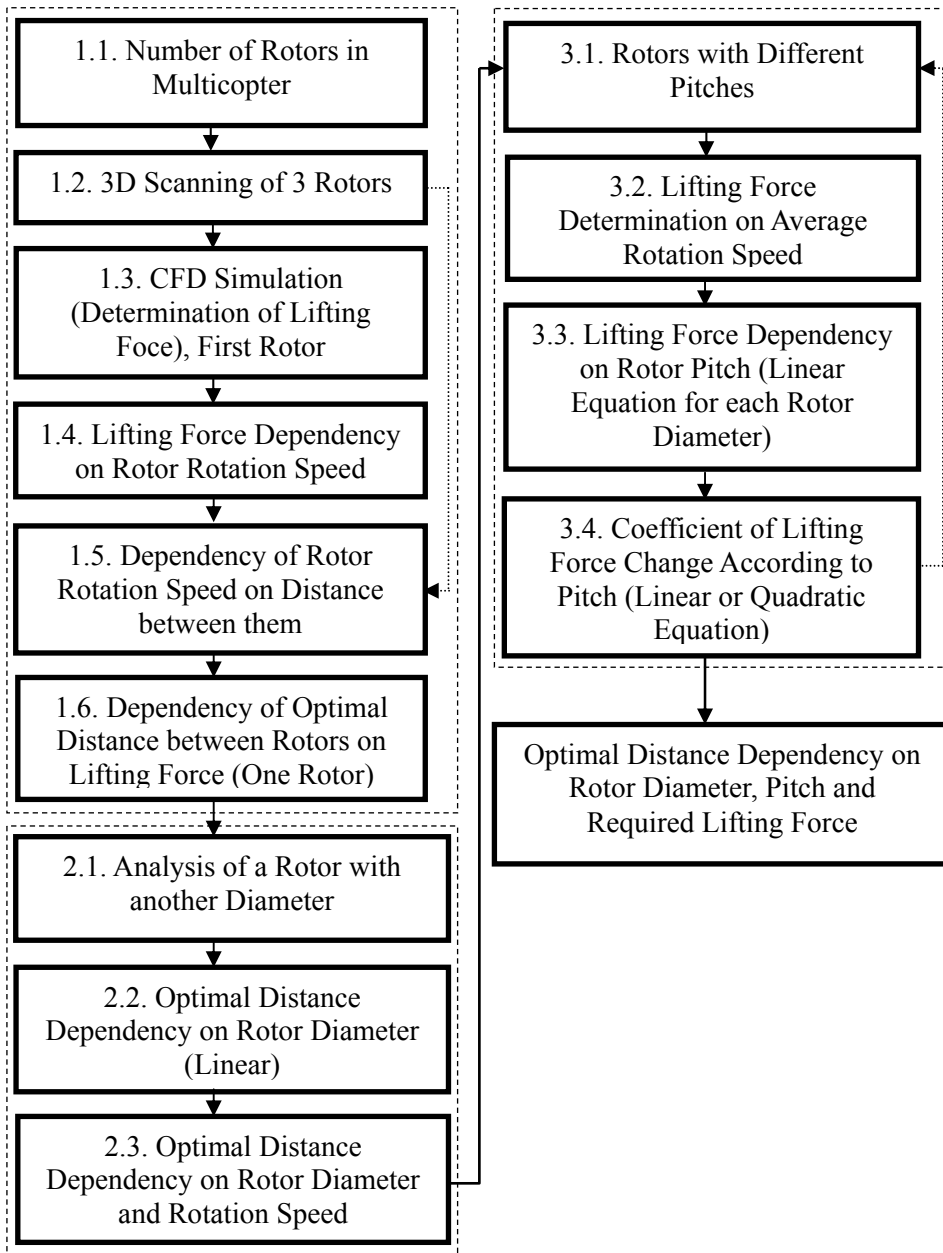


Figure 67. Determination of optimal distance between the rotors in the multicopter.

# CONCLUSIONS

## Results

One of the main objectives of this work was to develop a methodology for the optimization of the multicopter's propeller placement by changing rotor combinations and location for energy saving. Different methods of multicopters design were tested in terms of energy consumption using a combination of CFD simulations and experiments. Such efforts like coaxial rotor placement and shrouded rotors with the use of store bought propellers were examined.

Validity of the results obtained by CFD software SolidWorks Flow Simulation was confirmed, with the maximum difference of 3 %, as compared to the experiments on the simulations of separately standing rotors. The effects of rotor pitch on the lifting forces for different rotor diameters were studied. The methodology for determination of rotor pitch impact on the rotor lifting force was developed.

Numerous studies cover power consumption and optimization of coaxial rotor pairs, but no research has been reported on the influence of changing rotor size in pair. In fact, coaxial rotors consume more energy than separately standing propellers. Two coaxial rotors with the same size produce 21 % less lifting force because the upper rotor creates around 70 % of the total lifting force created by the rotor pair. When the upper rotor is larger than the lower one, the rotor placement becomes more efficient and vice versa. In a coaxial rotor pair, the flow from an upper rotor partly compensates the pressure difference near the lower rotor and leads to the reduction of the total lifting forces.

Shrouded rotors (covered with a shroud in the form of a cylindrical tube), commonly used for safety reasons, were checked for their influence on the motor energy consumption. With the increase of the shroud diameter, the lifting force also increases (energy consumption falls) until the moment when the rotor is working as separately standing. Motor power consumption of the shrouded rotor is higher than that fully opened. The reason is that these shrouds have a relatively large clearance between the rotor ends and the shroud because of their non-stiff design. This clearance does not allow them to work similarly to the impeller where vortexes near the rotor ends would be minimized and pressure difference adjustment near the upper and lower propeller faces would be avoided.

One of the most optimal variants from platforms with 3, 4, 6 and 8 rotors is a quadcopter – a four-rotor helicopter. Multicopters with six and eight rotors consume accordingly 3 % and 8 % more energy than a four rotor helicopter.

When the rotors in the quadrotor helicopter are very close to each other, flows from them hardly affect neighboring rotors and their motor power consumption. On large distances, the mass and dimensions between the rotors of a helicopter increase because of the lengthening of the central cross. No studies have been reported regarding the determination of an optimal distance between the rotors

in multicopters. Commonly, relatively large distances are used that affect the overall vehicle mass. A methodology for the optimization of the distance between the rotors in a multicopter was developed where the described sequence and types of activities must be done. As a result, a pair of equations was defined and an optimal distance between the studied rotors can be determined knowing the rotor diameter, pitch and overall mass of a multicopter. Building a multicopter with a distance calculated using the resulting equations flight duration can be increased up to 10 %.

The main conclusions are as follows:

1. The methodology for the determination of the optimal distance between the rotors in the multicopter for energy saving was developed. This methodology allows us to obtain the distance knowing the rotor diameter, pitch and overall mass of the multicopter.
2. Dependence of the lifting force of the coaxial rotor pair on the changes of propeller sizes in pair was found. It is shown that with the upper rotor larger than the lower one, the efficiency of the rotor pair is higher and vice versa.
3. The influence of the safety shroud on the propeller lifting force was determined. It is demonstrated that the efficiency of the shrouded rotors having relatively large clearance between the shroud and the rotor ends is lower than the efficiency of fully opened rotors.
4. Guidelines were developed to find the optimal number of rotors in the multicopter in terms of energy consumption. It is shown that one of the most optimal variants is the quadcopter.

## **Novelty**

- A new effective and robust methodology for the determination of the optimal distance between the rotors in the multicopter was developed considering the multicopter mass, rotor diameter and pitch as the parameters.
- New simulations were developed and a detailed analysis was made how coaxial rotor sizes in pair affect the total lifting force and an efficient rough simulation technique is proposed for solving similar tasks.
- Influence of the height and diameter of the shrouds around the rotors on motor energy consumption was analyzed and instructions for optimal parameter choice are given.



## **Future research**

The methodology described in this thesis suggests making a number of simulations for the determination of the optimal distance between the rotors. Each CFD simulation takes hours of computational time and it would be appropriate to decrease the number of those simulations. Using the developed methodology it is necessary to make calculations for some quantity of rotors with different blade profiles. In the analysis of the results it is required to find additional dependencies for decreasing the number of simulations in the methodology to determine an optimal distance.

To save energy in UAVs, use of shrouded rotors may be prospective. Theoretically they are more efficient than opened ones. Today's shrouds for the lifting force and optimization of energy consumption are not suitable for mini multicopters due to their mass and design stiffness. To improve the efficiency it is required to study the influence of the distance between the rotor blade tips and the shroud. Changing shroud geometry and design is also possible to optimize an aerial vehicle. It is recommended to study internal surface configurations of the shroud.

Coaxial rotor pairs commonly used in multicopters have separate motor for each rotor in pair that increases energy consumption of the whole system. It is recommended to study energy consumption of the rotor pair that uses one motor and the reversing mechanism for one rotor.

## REFERENCES

- [1] Ollero A., Merino L., Control and perception techniques for aerial robotics, *Annual Reviews in Control*, 2004, Vol. 28, 167 – 178.
- [2] Civilian applications: the challenges facing the UAV industry, *Air & Space Europe*, September – December 1999, Vol. 1 – 5, No. 6, 63 – 66.
- [3] Herrick K., Development of the unmanned aerial vehicle market: forecasts and trends, *Air & Space Europe*, March – April 2000, Vol. 2, No. 2, 25 – 27.
- [4] Erbil M. A., Prior S. D., Karamanoglu M., Odedra S., Barlow C., Lewis D., Reconfigurable unmanned aerial vehicles, *Proceedings of the International Conference on Manufacturing and Engineering Systems*, 2009, 392 – 421.
- [5] Current and future UAV military users and applications, *Air & Space Europe*, September – December 1999, Vol. 1 – 5, No. 6, 51 – 58.
- [6] Finn R. L., Wright D., Unmanned aircraft systems: Surveillance, ethics and privacy in civil applications, *Computer Law & Security Review*, 2012, Vol. 28, 184 – 194.
- [7] Girard A. R., Howell A. S., Hedrick J.K., Border patrol and surveillance missions using multiple unmanned air vehicles, *Proceedings of the 43rd IEEE Decision and Control*, Atlantis, Bahamas, 14 – 17 December, 2004, 620 – 625.
- [8] Coifman B., McCord M., Mishalani R. G., Iswalt M., Ji, Roadway traffic monitoring from an unmanned aerial vehicle, *IEE Proceedings Intelligent Transport Systems*, 2006, Vol. 153, No. 1, 11 – 20.
- [9] Ryan A., Hedrick J. K., A mode-switching path planner for UAV-assisted search and rescue, *Proceedings of the 44th IEEE Conference on Decision and Control*, Seville, Spain, 12 – 15 December, 2005, 1471 – 1476.
- [10] Casbeer D. W., Kingston D. B., Beard R. W., McLain T. W., Cooperative forest fire surveillance using a team of small unmanned air vehicles, *International Journal of Systems Science*, 2006, Vol. 37, No. 6, 351 – 360.
- [11] Xiaofeng L., Zhongren P., Liye Z., Li L., Unmanned Aerial Vehicle Route Planning for Traffic Information Collection, *Journal of Transportation Systems Engineering and Information Technology*, February 2012, Vol. 12, No. 1, 91 – 96.
- [12] Puri A., A survey of Unmanned Aerial Vehicles (UAV) for traffic surveillance, *Department of Computer Science and Engineering*, University of South Florida, 2008.

- [13] Courbon J., Mezouar Y., Guénard N., Martinet P., Vision-based navigation of unmanned aerial vehicles, *Control Engineering Practice*, July 2010, Vol. 18, No. 7, 789 – 799.
- [14] Yasir M., Azman A. W., Akbar F., Indoor UAV Positioning Using Stereo Vision Sensor, *Procedia Engineering*, 2012, Vol. 42, 575 – 579.
- [15] Xiang H., Tian L., Development of a low-cost agricultural remote sensing system based on an autonomous unmanned aerial vehicle (UAV), *Biosystems Engineering*, February 2011, Vol. 108, No. 2, 174 – 190.
- [16] Lin F., Chen B.M., Lum K.Y., Integration and implementation of a low-cost and vision UAV tracking system, *Proceedings of 26th Chinese Control Conference*, Zhangjiajie, China, 2007, 731 – 736.
- [17] Mejias L., Saripalli S., Campoy P., Sukhatme G.S., Visual servoing of an autonomous helicopter in urban areas using feature tracking, *Field Robotics*, 2006, Vol. 23, 185 – 199.
- [18] Sharp C.S., Shakenia O., Sastry S., A vision system for landing an unmanned aerial vehicle, *Proceedings of IEEE international conference on robotics and automation*, Seoul, Korea, 2001, 1720 – 1727.
- [19] Peng K., Cai G., Chen B. M., Dong M., Luma K. Y., Lee T. H., Design and implementation of an autonomous flight control law for a UAV helicopter, *Automatica*, 2009, Vol. 45, 2333 – 2338.
- [20] Civita M., Messner W.C., Kanade T., Modeling of small-scale helicopters with integrated first-principles and system-identification techniques, *Proceedings of 58th Forum of American Helicopter Society*, Montreal, Canada, 2002, 2505 – 2516.
- [21] Shim D.H., Kim H.J., Sastry S., Control system design for rotorcraft-based unmanned aerial vehicle using time-domain system identification, *Proceedings of IEEE Conference on Control Applications*, Anchorage, Alaska, USA, 2000, 808 – 813.
- [22] Johnson E.N., Kannan S.K., Adaptive trajectory control for autonomous helicopters, *AIAA Guidance Control Dynamics*, 2005, Vol. 28, 524 – 538.
- [23] Paw Y. C., Balas G. J., Development and application of an integrated framework for small UAV flight control development, *Mechatronics*, 2011, Vol. 21, 789 – 802.
- [24] Yueneng Y., Wu J., Zheng W., Variable structure attitude control for an UAV with parameter uncertainty and external disturbance, *Procedia Engineering*, 2011, Vol. 15, 408 – 415.
- [25] Andersh J., Mettler B., System integration of a miniature rotorcraft for aerial tele-operation research, *Mechatronics*, 2011, Vol. 21, 776 – 788.

- [26] Funaki M., Hirasawa N., Outline of a small unmanned aerial vehicle (Ant-Plane) designed for Antarctic research, *Polar Science*, 2008, Vol. 2, 129 – 142.
- [27] Dittrich J.S., Johnson E.N., Multi-sensor navigation system for an autonomous helicopter, *Proceedings of 21st digital avionics systems conference*, Irvine, California, 2002, 1 – 19.
- [28] [http://www.tealgroup.com/index.php?option=com\\_content&view=article&id=66:teal-group-forecasts-38-growth-in-leo-satellites-for-2010-2014&catid=3&Itemid=16](http://www.tealgroup.com/index.php?option=com_content&view=article&id=66:teal-group-forecasts-38-growth-in-leo-satellites-for-2010-2014&catid=3&Itemid=16), 09.2012.
- [29] Longest flight for small UAV using Protonex fuel cell, *Fuel Cells Bulletin*, January 2008, Vol. 1, 5.
- [30] Frulla G., Cestino E., Design, manufacturing and testing of a HALE-UAV structural demonstrator, *Composite Structures*, 2008, Vol. 83, 143 – 153.
- [31] Gavrillets V., Shterenberg A., Dahleh M.A., Feron E., Avionics system for a small unmanned helicopter performing aggressive maneuvers, *Proceedings of 19th Digital Avionics Systems Conference*, Philadelphia, USA, 2000, 1 – 7.
- [32] Mettler B., *Identification modeling and characteristics of miniature rotorcraft*, Norwell, MA, Kluwer Academic Publishers, 2003.
- [33] Dong M., Chen B.M., Cai G., Peng K., Development of a real-time onboard and ground station software system for a UAV helicopter, *Aerospace Computing, Information and Communication*, 2007, Vol. 4, 933 – 955.
- [34] Taha Z., Tang Y.R., Yap K.C., Development of an onboard system for flight data collection of a small-scale UAV helicopter, *Mechatronics*, 2011, Vol. 21, 132 – 144.
- [35] Musial M., Brandenburg U.M., Hommel G., Inexpensive system design: The flying robot Marvin, *Proceedings of 6th international UAVs Conference on Unmanned Air Vehicle Systems*, Bristol, UK, 2001, 1 – 12.
- [36] Yoo D., Oh H., Won D., Tahk M., Dynamic modeling and stabilization techniques for tri-rotor unmanned aerial vehicles, *International Journal of Aeronautical & Space Science*, 2010, Vol. 11, No. 3, 167 – 174.
- [37] <http://www.braunmod.de/etribelle.htm>, 09.2011.
- [38] Salazar-Cruz S., Lozano R., Escaren J., Stabilization and nonlinear control for a novel trirotor mini-aircraft, *Control Engineering Practice*, 2009, Vol. 17, 886 – 894.
- [39] Pounds P., Mahony R., Corke P., Modelling and control of a large quadrotor robot, *Control Engineering Practice*, 2010, Vol. 18, 691 – 699.

- [40] Hoffmann G. M., Huang H., Waslander S. L., Tomlin C. J., Precision flight control for a multi-vehicle quadrotor helicopter test bed, *Control Engineering Practice*, 2011, Vol. 19, 1023 – 1036.
- [41] Derafa L., Benallegue A., Fridman L., Super twisting control algorithm for the attitude tracking of a four rotors UAV, *Journal of the Franklin Institute*, 2012, Vol. 349, 685 – 699.
- [42] Hoffmann G.M., Huang H., Waslander S.L., Tomlin C.J., Quadrotor helicopter flight dynamics and control: theory and experiment, *AIAA Guidance, Navigation and Control Conference and Exhibit*, Hilton Head, South Carolina, 2007, 1 – 20.
- [43] Lee J., Yoo C., Park Y., Park B., Lee S., Gweon D., Chang P., An experimental study on time delay control of actuation system of tilt rotor unmanned aerial vehicle, *Mechatronics*, 2012, Vol. 22, 184 – 194.
- [44] Haixu L., Xiangju Q., Weijun W., Multi-body Motion Modeling and Simulation for Tilt Rotor Aircraft, *Chinese Journal of Aeronautics*, 2010, Vol. 23, 415 – 422.
- [45] Cetinsoy E., Dikyar S., Hancer C., Oner K.T., Sirimoglu E., Unel M., Aksit M.F., Design and construction of a novel quad tilt-wing UAV, *Mechatronics*, 2012, Vol. 22, 723 – 745.
- [46] Ansari S.A., Bikowski R. Z, Aerodynamic modelling of insect-like flapping flight for micro air vehicles, *Progress in Aerospace Sciences*, 2006, Vol. 42, 129 – 172.
- [47] Song Y. D., Weng L., Lebby G., Human memory/learning inspired control method for flapping-wing micro air vehicles, *Journal of Bionic Engineering*, 2010, Vol. 7, 127 – 133.
- [48] J. T. K. Ping, C. S. Tan, V. O. T. Tat, Coanda effect test bench (CoETB) – design enhancement of the coanda JLT craft, *IEEE Conference on Sustainable Utilization and Development in Engineering and Technology*, 2011, 25 – 30.
- [49] Denisov S., *Coanda Effect, Index of Physical Phenomena and Effects*, Obinsk, 1979.
- [50] <http://www.meridian-int-res.com>, 10.2011.
- [51] Gebauer J., Koci P., Sofer P., Multicopter potentialities, *13th International Carpathian Control Conference*, 2012, 194 – 197.
- [52] Jasim A., Duque E., Helicopter rotor blade computation in unsteady flows using moving overset grids, *Journal of Aircraft*, 1996, Vol. 33, No. 1, 54 – 60.
- [53] Yongjie S., Qijun Z., Feng F., Guohua X., A new single-blade based hybrid CFD method for hovering and forward-flight rotor computation, *Chinese Journal of Aeronautics*, 2011, Vol. 24, 127 – 135.

- [54] Ryan S.A., *Design and optimisation of a propeller for a micro air vehicle using computational fluid dynamics*, Thesis, University of New South Wales at the Australian Defence Force Academy, 2010, 17 – 23.
- [55] Rashahmadi S., Abbaszadeh M., Hoseyni S., Alizadeh R., Design of a constant chord single-rotating propeller using lock and goldstein techniques, *World Academy of Science, Engineering and Technology*, 2011, Vol. 56, 1585 – 1589.
- [56] Brocklehurst A., Barakos G.N., A review of helicopter rotor blade tip shapes, *Progress in Aerospace Sciences*, 2013, Vol. 56, 35 – 74.
- [57] Pape A., Beaumier P., Numerical optimization of helicopter rotor aerodynamic performance in hover, *Aerospace Science and Technology*, 2005, Vol. 9, 191 – 201.
- [58] Beaumier P., Costes M., Gaveriaux R., Comparison between FP3D full potential calculations and S1 Modane wind tunnel test results on advanced fully instrumented rotors, *Nineteenth European Rotorcraft Forum*, Como, Italy, 1993, 142 – 155.
- [59] Bohorquez F., *Rotor hover performance and system design of an efficient coaxial rotary wing micro air vehicle*, Thesis, University of Maryland, 2007.
- [60] Heyong X., Zhengyin Y., Numerical simulation of unsteady flow around forward flight helicopter with coaxial rotors, *Chinese Journal of Aeronautics*, 2011, Vol. 24, 1 – 7.
- [61] Bell J., Brazinskas M., Prior S., Optimizing performance variables for small unmanned aerial vehicle co-axial rotor systems, *School of Engineering and Information Sciences*, Middlesex University, 2011, 1 – 10.
- [62] Wei Z., Ningjun F., Zhengjie W., Yanxuan W., Modeling and aerodynamic analysis of a ducted-fan micro aerial vehicle, *Modelling, Identification and Control*, Wuhan, China, 24 – 26 June 2012, 768 – 773.
- [63] Gebauer J., Koci P., Measurements of features of the ducted fan as a possible actuator of a multi-copter vehicle, *12th International Carpathian Control Conference (ICCC)*, 2011, 127 – 130.
- [64] Zhao J., Hou Q., Jin H., Zhu Y., Li G., CFD analysis of ducted-fan UAV based on magnus effect, *Proceedings of IEEE International Conference on Mechatronics and Automation*, 5 – 8 August, 2012, China, 1722 – 1726.
- [65] Haikin S., Kutta–Joukowski theorem, *Physical Fundamentals of Mechanics*, Moscow, 1971.
- [66] Zagordan A. M., *Elementary Theory of Helicopter*, Moscow, 1955.

- [67] Aleksandrov V., Air propeller working principle, *Air Propellers*, Moscow, 1951, 10 – 22.
- [68] <http://www.rc-airplane-world.com/propeller-size.html>, 10.2012.
- [69] [http://www.pilotfriend.com/training/flight\\_training/fxd\\_wing/props.htm](http://www.pilotfriend.com/training/flight_training/fxd_wing/props.htm), 10.2012.
- [70] Wald Q. R., The aerodynamics of propellers, *Progress in Aerospace Sciences*, 2006, Vol. 42, 85 – 128.
- [71] Strawn R., Caradonna F., Duque E., 30 years rotorcraft computational fluid dynamics research and development, *Journal of the American Helicopter Society*, 2006, Vol. 51, No. 1, 5 – 21.
- [72] Kang H., Kwon O., Unstructured mesh Navier-Stokes calculations of the flow field of a helicopter rotor in hover, *Journal of the American Helicopter Society*, 2002, 1 – 10.
- [73] The Navier-Stokes equations for laminar and turbulent fluid flows *SolidWorks Flow Simulation*, Dassault Systems, 2012, 1.1 – 1.52.
- [74] Bangalore A., Sankar L., Forward-flight analysis of slatted rotors using Navier-Stokes methods, *Journal of Aircraft*, January – February 1997, Vol. 34, No. 1, 80 – 86.
- [75] Batchelor G., *An Introduction to Fluid Dynamics*, 1967, 137 – 142.
- [76] <http://www.navier-stokes.net/nsfield.htm>, 04.2013.
- [77] [http://www.allaboutcircuits.com/vol\\_1/chpt\\_9/7.html](http://www.allaboutcircuits.com/vol_1/chpt_9/7.html), 07.2013.
- [78] <http://www.rc-airplane-world.com/propeller-size.html>, 10.2012.
- [79] [http://www.pilotfriend.com/training/flight\\_training/fxd\\_wing/props.htm](http://www.pilotfriend.com/training/flight_training/fxd_wing/props.htm), 10.2012.
- [80] Trofimova T. I., *Course of Physics*, 2004, 34 – 39.
- [81] Rand O., Khromov V., Aerodynamic optimization of coaxial rotor in hover and axial flight, *27th International Congress of the Aeronautical Sciences*, 19 – 24 September 2010, Nice, France, 1 – 13.
- [82] K. U. Lee, Y. H. Yun, W. Chang, J. B. Park, Y. H. Choi, Modeling and altitude control of quad-rotor UAV, *11th International Conference on Control, Automation and Systems*, Korea, 2011, 1897 – 1902.
- [83] B. Chowdhury, A. Kulhare, G. Raina, A generalized control method for a tilt-rotor UAV stabilization, *Proceedings of the 2012 IEEE International Conference on Cyber Technology in Automation, Control and Intelligent Systems*, Thailand, 309 – 314.

## OTHER PUBLICATIONS

1. Aleksandrov, D., Penkov, I., Rotor lifting force optimization by changing dimensions of rim around it, *13th International Symposium, Topical Problems in the Field of Electrical and Power Engineering, Doctoral School of Energy and Geotechnology II*, Pärnu, 14 – 19 January 2013, 292 – 295.
2. Aleksandrov, D., Penkov, I., Optimization mini unmanned helicopter energy consumption by changing geometrical parameters of coaxial rotor pairs, *12th International Symposium Topical Problems in the Field of Electrical and Power Engineering, Doctoral School of Energy and Geotechnology II*, Kuressaare, Estonia, 11 – 16 June 2012, 139 – 141.
3. Aleksandrov, D., Penkov, I., Energy consumption of mini UAV helicopters with different number of rotors, *11th International Symposium Topical Problems in the Field of Electrical and Power Engineering, Doctoral School of Energy and Geotechnology II*, Pärnu, Estonia, 16 – 21 January 2012, 259 – 262.
4. Aleksandrov, D., Penkov, I., Energy saving types of mini UAV, *9th International Symposium Topical Problems in the Field of Electrical and Power Engineering, Doctoral School of Energy and Geotechnology II*, Pärnu, Estonia, 14 – 19 June 2010, 117 – 120.
5. Aleksandrov, D., Penkov, I., Fluid flow optimization on semiautomatic code marker base, *8th International Symposium Topical Problems in the Field of Electrical and Power Engineering, Doctoral School of Energy and Geotechnology II*, Pärnu, Estonia, 11 – 16 January 2010, 306 – 308.



## ACKNOWLEDGEMENTS

I would like to thank everyone who helped and supported me through the process of learning. Also want to thank my relatives and friends for their support and understanding.

Special thanks to:

- Igor Penkov, Associate Professor, Faculty of Mechanical Engineering, Department of Mechatronics, Chair of Mechanosystem Components, TUT, Thesis Supervisor.
- Mart Tamre, Professor, Faculty of Mechanical Engineering, Department of Mechatronics, Chair of Mechatronics Systems, TUT.
- Trieu Minh Vu, Professor, Faculty of Mechanical Engineering, Department of Mechatronics, Chair of Mechanosystem Components, TUT.
- Merle Randrüüt, Associate Professor, Faculty of Mechanical Engineering, Department of Mechatronics, Chair of Mechatronics Systems, TUT.
- Toomas Kübarsepp, Professor, Faculty of Mechanical Engineering, Department of Mechatronics, Chair of Quality Engineering and Metrology, TUT.
- Mare-Anne Laane, Lecturer, School of Economics and Business Administration, Department of Business Administration, Chair of Marketing.
- Jess Frandsen, CEO, PLM Group ApS.
- Silva Lill, CMO, PLM Group ApS.

I would like to thank all organizations for financial support of this study:

- Estonian Ministry of Education and Research (Project SF0140113BS08 „Mechatronic and Production Systems Proactivity and Behavioural Models“).
- European Social Fund (Project "Doctoral School of Energy and Geotechnology II") Archimedes Foundation.
- ESF DoRa T8 Funding, Archimedes Foundation.

## **ABSTRACT**

In the last decades UAVs (Unmanned Aerial Vehicles) have generated great interest in industrial and academic circles because they are capable of carrying out work under conditions where the surrounding environment is dangerous or not available to humans. The range of applications performed by UAVs is wide, such as police, rescue and firefighter needs, research, cinematography and other spheres. UAVs have exclusive capabilities like hovering, vertical takeoff and landing, limited launching spaces and good maneuvering.

Presently mini aerial vehicles are using standard power sources and their flight duration is very low in terms of actual needs. The aim of this work was to decrease energy consumption of multicopter by changing locations and configurations of rotors available on the market.

This thesis consists of six parts: introduction, an overview of current UAVs, evaluation of one rotor lifting force, calculations of lifting force of different rotor placement schemes, determination of optimal distance between rotors and the conclusion. The Introduction describes the sphere of use and the value of unmanned aerial vehicles in the industries. Literature is reviewed and flying types and design of existing mini UAVs are described. Articles reporting research for the optimization of propellers and their usage in multicopters are reviewed.

Firstly, one rotor's lifting force was determined using CFD (Computational Fluid Dynamics) simulation and compared with experiments. Experiments were made on a special testing device to measure the lifting force, angular velocity and power consumption. The validity of CFD simulations was confirmed, with a maximum difference of 3 % (compared experiments). It was found that changing rotor pitch affects the lifting force linearly. Based on results, the pitch correction coefficient was calculated.

Popular coaxial rotor layouts were tested with different rotor sizes in pair. This placement of rotors has benefits in a tricopter setup but consumes much more energy than separately standing rotors. Two coaxial rotors with the same size produce about 21 % less lifting force because the flow from the upper rotor partly compensates the pressure difference near the lower rotor. Shrouded rotors (covered with a shroud), commonly used for safety reasons, were checked for influence on a motor's energy consumption. Theoretically, they consume less energy than opened rotors, but in practice it is vice versa. The reason is that the shrouds that are used for safety benefits have a relatively large clearance between the rotor ends because of their non-stiff design. Based on previous simulations and experiment results, theoretical flight duration of multicopters with different numbers of propellers was calculated. One of the most optimal variants from platforms with 3, 4, 6 and 8 rotors is quadcopter – a four rotor helicopter.

To determine an optimal distance between the quadrotor helicopter rotors, CFD simulations were used and were proved by experiments. Dependency of an

optimal distance on the lifting force can be presented as a pair of equations. Using them it is possible to find the optimal distance between the rotors (model of a rotor used in calculations) in a quadrocopter, knowing the rotor pitch, diameter and overall mass of the vehicle. The methodology of the determination of the optimal distance between the propellers in the multicopter was developed. Building a quadrocopter with a distance calculated using the presented methodology flight duration can be increased up to 10 %.

This doctoral thesis describes different efforts to expand mini UAV helicopter flight duration. Results show that not all ways of rotor usage are optimal and give long lasting flights. Recommendations for the design of the multicopter are presented. The presented methodology enables the determination of the optimal distance between the rotors in multi-rotor helicopters.

## KOKKUVÕTE

Viimasel ajal on mehitamata õhusõidukid (ing. UAVs – *Unmanned Aerial Vehicles*) tekitanud suurt huvi nii tööstus- kui ka akadeemilistes ringkondades tänu nende võimalusele teha tööd tingimustes, kus ümbritsev keskkond on ohtlik või ei ole ligipääsetav inimestele. UAV kasutusala on väga lai, eelkõige politsei, pääste ja tuletõrje operatsioonidel. Lisaks on võimalik neid kasutada teadustöös, kinematograafias ja paljudes muudes valdkondades. UAV ühendab unikaalseid võimalusi, nagu hõljumine, vertikaalne õhkutõus ja maandumine raskesti ligipääsetavatesse kohtadesse, loomulikult ka hea manööverdamisvõime.

Tänapäeva väikesed mehitamata õhusõidukid kasutavad tavaliselt standardseid energiaallikaid ja nende lennukestvus on väike võrreldes reaalsete vajadustega. Käesoleva töö eesmärk on multikopteri propellerite asukoha ja kasutamispõhimõtte optimeerimise meetodika arendamine (muutes standardsete rootorite asukohti ja konfiguratsioone) energiatarbimise vähendamise eesmärgil.

Dissertatsioon koosneb viiest osast: sissejuhatus; ühe rootori tõstejõu määramine; tõstejõu määramine, kasutades erinevaid rootori paigalduse skeeme; optimaalse vahekauguse määramine propellerite vahel; kokkuvõte. Sissejuhatuses kirjeldatakse mehitamata kergklassi multikopterite kasutusala ulatust ja nende tänapäevast tähtsust. Analüüsitakse kirjandust, tuuakse välja olemasolevate mehitamata kergklassi multikopterite tüübid ja konstruktsioonid ning kuidas neid tänapäeval arendatakse. Antakse ülevaade artiklitest, mis käsitlevad rootorite optimeerimist ja nende kasutusprintsippe multikopterites.

Esimesed arvutused tehti ühe rootori tõstejõu määramiseks, kasutades CFD (*Computational Fluid Dynamics*) tarkvara ning tulemusi võrreldi reaalsete eksperimentidega. Reaalsed eksperimendid viidi läbi spetsiaalselt käesoleva ülesande jaoks ehitatud katsestendil, kus oli võimalus mõõta tõstejõudu, nurkkiirust ja energiatarbimist. Tulemuste võrdlemine näitas, et CFD simulatsiooni tulemus on usaldusväärne ja maksimaalne erinevus on ligikaudu 3% (võrreldes reaalse eksperimendiga). Tulemused näitasid, et muutes rootori sammu, muutub selle tõstejõud lineaarselt. Vastavalt saadud tulemustele arvatati rootori sammu korrigeerimise koefitsient.

Populaarse koaksiaalse rootori paigalduse skeemi katsetati, kasutades erineva suurusega propellereid paaris. Selline rootori paigalduse skeem omab eeliseid kolme rootoriga lendava platvormi puhul, aga tarbib rohkem energiat kui eraldi seisvad rootorid. Kaks samasugust propellerit koaksiaalses paaris tekitavad 21% vähem tõstejõudu, kuna ülemise rootori õhuvool kompenseerib osaliselt rõhuerinevuse alumise rootori juures. Kui ülemine rootor on alumisest suurem, siis on süsteemi üldefektiivsus väiksem ja vastupidi. Rotorite puhul kasutatakse ka tihti turvaümbrist (rootorid on paigaldatud ümmarguse ümbrise sisse) ning käesoleva töö raames kontrolliti ka nende energiatarbimist. Teoreetiliselt tarbivad nad vähem energiat, võrreldes avatud rootoritega, aga praktikas on vastupidi. Põhjus on selles, et turvaümbrise ja rootori vahele jääb

suhteliselt suur vahe konstruktsiooni iseärasuse tõttu. Tuginedes arvutuslikele (CFD) ja reaalsele tulemustele, koostati teoreetilise lennu kestvuse võrdlus erineva arvu rootoriga multikopteritele. Üks kõige optimaalsematest multikopteritest on kvadrokopter – helikopter nelja rootoriga.

Optimaalse vahekauguse määramiseks nelja rootoriga helikopteri propellerite vahel kasutati CFD-analüüsi, mida kontrolliti ja tõestati reaalse katsetega. Optimaalne vahekaugus kvadrokopteri propellerite vahel (identsete propellerite korral) on leitav töös esitatud kahe valemi lahendusest, kus rootori diameeter, rootoriga samm ja kopteri mass on parameetrid. Potentsiaalselt võib multikopteri lennupikkust suurendada kuni 10%, kasutades optimaalset rootoriga vahelist kaugust. Töötati välja propellerite optimaalse vahekauguse leidmise meetodika.

Doktoritöös on kirjeldatud ka erinevaid eksperimente lennu kestvuse pikendamiseks mehitamata õhusõiduki jaoks. Tulemused näitavad, et kõik propellerite kasutusvõimalused ei ole optimaalsed ning seega ei garanteeri pikaajalist lennu. Esitatakse soovitusi multikopteri konstrueerimiseks. Uus meetodika võimaldab leida multikopteri optimaalse rootoriga vahelise kauguse.

#### Põhjäreldused

1. Töötati välja meetodika rootoriga optimaalse vahekauguse leidmiseks eesmärgiga vähendada energiatarbimist. Kasutades seda meetodikat, on võimalik leida vahekaugust teades rootori diameeter, samm ja kvadrokopteri mass.
2. Leiti koaksiaalse rootori paari tõstejõu sõltuvus rootori suuruse muutusest. Kui ülemine rootor on alumisest suurem, siis süsteemi üldefektiivsus on väiksem ja vastupidi.
3. Määrati turvaümbrise mõju rootori tõstejõule. Turvaümbrisega kaetud rootori (kus on kasutatud suhteliselt suurt vahet propelleri otste ja ümbrise vahel) energiatarbimine on suurem kui täiesti avatud rootoriga.
4. Töötati välja juhend optimaalse rootoriga arvu leidmiseks eesmärgiga vähendada energiatarbimist. On näidatud, et üks kõige optimaalsematest multikopteritest on kvadrokopter – helikopter nelja rootoriga.

# CURRICULUM VITAE

## 1. Personal data

Name: Dmitri Aleksandrov  
Date and place of birth: 18 August 1986, Estonia  
Citizenship: Estonia  
E-mail address: dmitri.aleksandrov@gmail.com

## 2. Education

Educational institution	Graduation year	Education (field of study/degree)
Tallinn University of Technology	2007	B.Sc. in Mechatronics
Tallinn University of Technology	2009	M.Sc. in Mechatronics

## 3. Language competence/skills (fluent, average, basic skills)

Language	Level
Russian	native
Estonian	fluent
English	fluent

## 4. Professional employment

Period	Organisation	Position
2006 – 2007	DesFactory OÜ	Mechanical Designer
2007 – ...	PLM Group Eesti OÜ	Project Manager

## 5. Research activity, including honours and thesis supervised

SolidWorks Elite Application Engineer 2011 (highest SolidWorks award)

# ELULOOKIRJELDUS

## 1. Isikuandmed

Ees- ja perekonnanimi: Dmitri Aleksandrov  
Sünniaeg ja -koht: 18. august 1986, Eesti  
Kodakondsus: Eesti  
E-posti aadress: dmitri.aleksandrov@gmail.com

## 2. Hariduskäik

Õppeasutus (nimetus lõpetamise ajal)	Lõpetamise aeg	Haridus (eriala/kraad)
Tallinna Tehnikaülikool	2007	Mehhatroonika, Bakalaureusekraad
Tallinna Tehnikaülikool	2009	Mehhatroonika, Magistrikraad

## 3. Keelteoskus (alg-, kesk- või kõrgtase)

Keel	Tase
Vene	emakeel
Eesti	kõrgtase
Inglise	kõrgtase

## 4. Teenistuskäik

Töötamise aeg	Tööandja nimetus	Ametikoht
2006 – 2007	DesFactory OÜ	Mehaanikaprojekterija
2007 – ...	PLM Group Eesti OÜ	Projektijuht

## 5. Teadustegevus, sh tunnustused ja juhendatud lõputööd

SolidWorks Elite Application Engineer 2011 (kõrgem SolidWorks autasu)

**DISSERTATIONS DEFENDED AT  
TALLINN UNIVERSITY OF TECHNOLOGY ON  
*MECHANICAL ENGINEERING***

1. **Jakob Kübarsepp**. Steel-Bonded Hardmetals. 1992.
2. **Jakub Kõo**. Determination of Residual Stresses in Coatings & Coated Parts. 1994.
3. **Mart Tamre**. Tribocharacteristics of Journal Bearings Unlocated Axis. 1995.
4. **Paul Kallas**. Abrasive Erosion of Powder Materials. 1996.
5. **Jüri Pirso**. Titanium and Chromium Carbide Based Cermets. 1996.
6. **Heinrich Reshetnyak**. Hard Metals Serviceability in Sheet Metal Forming Operations. 1996.
7. **Arvi Kruusing**. Magnetic Microdevices and Their Fabrication methods. 1997.
8. **Roberto Carmona Davila**. Some Contributions to the Quality Control in Motor Car Industry. 1999.
9. **Harri Annuka**. Characterization and Application of TiC-Based Iron Alloys Bonded Cermets. 1999.
10. **Irina Hussainova**. Investigation of Particle-Wall Collision and Erosion Prediction. 1999.
11. **Edi Kulderknup**. Reliability and Uncertainty of Quality Measurement. 2000.
12. **Vitali Podgurski**. Laser Ablation and Thermal Evaporation of Thin Films and Structures. 2001.
13. **Igor Penkov**. Strength Investigation of Threaded Joints Under Static and Dynamic Loading. 2001.
14. **Martin Eerme**. Structural Modelling of Engineering Products and Realisation of Computer-Based Environment for Product Development. 2001.
15. **Toivo Tähemaa**. Assurance of Synergy and Competitive Dependability at Non-Safety-Critical Mechatronics Systems design. 2002.
16. **Jüri Resev**. Virtual Differential as Torque Distribution Control Unit in Automotive Propulsion Systems. 2002.
17. **Toomas Pihl**. Powder Coatings for Abrasive Wear. 2002.
18. **Sergei Letunovitš**. Tribology of Fine-Grained Cermets. 2003.
19. **Tatyana Karaulova**. Development of the Modelling Tool for the Analysis of the Production Process and its Entities for the SME. 2004.
20. **Grigori Nekrassov**. Development of an Intelligent Integrated Environment for Computer. 2004.



21. **Sergei Zimakov.** Novel Wear Resistant WC-Based Thermal Sprayed Coatings. 2004.
22. **Irina Preis.** Fatigue Performance and Mechanical Reliability of Cemented Carbides. 2004.
23. **Medhat Hussainov.** Effect of Solid Particles on Turbulence of Gas in Two-Phase Flows. 2005.
24. **Frid Kaljas.** Synergy-Based Approach to Design of the Interdisciplinary Systems. 2005.
25. **Dmitri Neshumayev.** Experimental and Numerical Investigation of Combined Heat Transfer Enhancement Technique in Gas-Heated Channels. 2005.
26. **Renno Veinthal.** Characterization and Modelling of Erosion Wear of Powder Composite Materials and Coatings. 2005.
27. **Sergei Tisler.** Deposition of Solid Particles from Aerosol Flow in Laminar Flat-Plate Boundary Layer. 2006.
28. **Tauno Otto.** Models for Monitoring of Technological Processes and Production Systems. 2006.
29. **Maksim Antonov.** Assessment of Cermets Performance in Aggressive Media. 2006.
30. **Tatjana Barashkova.** Research of the Effect of Correlation at the Measurement of Alternating Voltage. 2006.
31. **Jaan Kers.** Recycling of Composite Plastics. 2006.
32. **Raivo Sell.** Model Based Mechatronic Systems Modeling Methodology in Conceptual Design Stage. 2007.
33. **Hans Rämmal.** Experimental Methods for Sound Propagation Studies in Automotive Duct Systems. 2007.
34. **Meelis Pohlak.** Rapid Prototyping of Sheet Metal Components with Incremental Sheet Forming Technology. 2007.
35. **Priidu Peetsalu.** Microstructural Aspects of Thermal Sprayed WC-Co Coatings and Ni-Cr Coated Steels. 2007.
36. **Lauri Kollo.** Sinter/HIP Technology of TiC-Based Cermets. 2007.
37. **Andrei Dedov.** Assessment of Metal Condition and Remaining Life of In-service Power Plant Components Operating at High Temperature. 2007.
38. **Fjodor Sergejev.** Investigation of the Fatigue Mechanics Aspects of PM Hardmetals and Cermets. 2007.
39. **Eduard Ševtšenko.** Intelligent Decision Support System for the Network of Collaborative SME-s. 2007.
40. **Rünno Lumiste.** Networks and Innovation in Machinery and Electronics Industry and Enterprises (Estonian Case Studies). 2008.

41. **Kristo Karjust.** Integrated Product Development and Production Technology of Large Composite Plastic Products. 2008.
42. **Mart Saarna.** Fatigue Characteristics of PM Steels. 2008.
43. **Eduard Kimmari.** Exothermically Synthesized B<sub>4</sub>C-Al Composites for Dry Sliding. 2008.
44. **Indrek Abiline.** Calibration Methods of Coating Thickness Gauges. 2008.
45. **Tiit Hindreus.** Synergy-Based Approach to Quality Assurance. 2009.
46. **Karl Raba.** Uncertainty Focused Product Improvement Models. 2009.
47. **Riho Tarbe.** Abrasive Impact Wear: Tester, Wear and Grindability Studies. 2009.
48. **Kristjan Juhani.** Reactive Sintered Chromium and Titanium Carbide-Based Cermets. 2009.
49. **Nadežda Dementjeva.** Energy Planning Model Analysis and Their Adaptability for Estonian Energy Sector. 2009.
50. **Igor Krupenski.** Numerical Simulation of Two-Phase Turbulent Flows in Ash Circulating Fluidized Bed. 2010.
51. **Aleksandr Hlebnikov.** The Analysis of Efficiency and Optimization of District Heating Networks in Estonia. 2010.
52. **Andres Petritšenko.** Vibration of Ladder Frames. 2010.
53. **Renee Joost.** Novel Methods for Hardmetal Production and Recycling. 2010.
54. **Andre Gregor.** Hard PVD Coatings for Tooling. 2010.
55. **Tõnu Roosaar.** Wear Performance of WC- and TiC-Based Ceramic-Metallic Composites. 2010.
56. **Alina Sivitski.** Sliding Wear of PVD Hard Coatings: Fatigue and Measurement Aspects. 2010.
57. **Sergei Kramanenko.** Fractal Approach for Multiple Project Management in Manufacturing Enterprises. 2010.
58. **Eduard Latõsov.** Model for the Analysis of Combined Heat and Power Production. 2011.
59. **Jürgen Riim.** Calibration Methods of Coating Thickness Standards. 2011.
60. **Andrei Surzhenkov.** Duplex Treatment of Steel Surface. 2011.
61. **Steffen Dahms.** Diffusion Welding of Different Materials. 2011.
62. **Birthe Matsi.** Research of Innovation Capacity Monitoring Methodology for Engineering Industry. 2011.
63. **Peeter Ross.** Data Sharing and Shared Workflow in Medical Imaging. 2011.
64. **Siim Link.** Reactivity of Woody and Herbaceous Biomass Chars. 2011.

65. **Kristjan Plamus**. The Impact of Oil Shale Calorific Value on CFB Boiler Thermal Efficiency and Environment. 2012.
66. **Aleksei Tšinjan**. Performance of Tool Materials in Blanking. 2012.
67. **Martinš Sarkans**. Synergy Deployment at Early Evaluation of Modularity of the Multi-Agent Production Systems. 2012.
68. **Sven Seiler**. Laboratory as a Service – A Holistic Framework for Remote and Virtual Labs. 2012.
69. **Tarmo Velsker**. Design Optimization of Steel and Glass Structures. 2012.
70. **Madis Tiik**. Access Rights and Organizational Management in Implementation of Estonian Electronic Health Record System. 2012.
71. **Marina Kostina**. Reliability Management of Manufacturing Processes in Machinery Enterprises. 2012.
72. **Robert Hudjakov**. Long-Range Navigation for Unmanned Off-Road Ground Vehicle. 2012.
73. **Arkadi Zikin**. Advanced Multiphase Tribo-Functional PTA Hardfacings. 2013.
74. **Alar Konist**. Environmental Aspects of Oil Shale Power Production. 2013.
75. **Inge Roos**. Methodology for Calculating CO<sub>2</sub> Emissions from Estonian Shale Oil Industry. 2013.
76. **Dmitri Shvarts**. Global 3D Map Merging Methods for Robot Navigation. 2013.
77. **Kaia Lõun**. Company's Strategy Based Formation of e-Workplace Performance in the Engineering Industry. 2013.